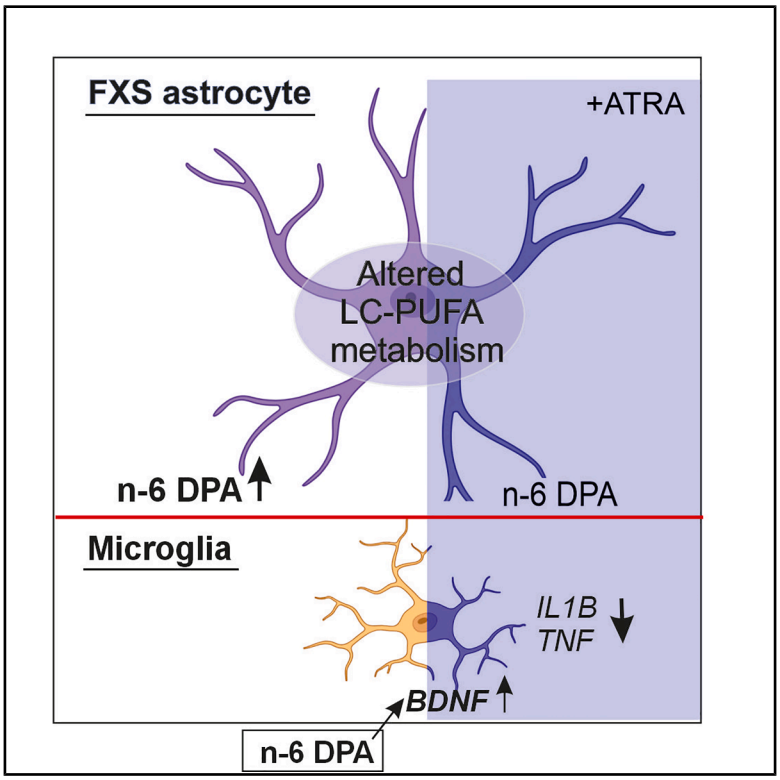
iScience

Article

Astrocytes contribute to long-chain polyunsaturated fatty acid metabolism affecting microglia in fragile X syndrome

Graphical abstract



Highlights

- Long-chain PUFA metabolism is dysregulated in human FXS iPSC-derived astrocytes
- Altered n-6/n-3 PUFA balance elevates secretion of n-6 DPA by FXS astrocytes
- Microglia supplemented with n-6 DPA exhibit increased *BDNF* and reduced *IL1B* expression
- ATRA attenuates n-6 DPA release by FXS astrocytes and the microglial pro-inflammatory state

Authors

Dmytro Gerasymchuk, Karo Talvio, Andrew H. House, ..., Jari Koistinaho, Reijo Käkelä, Maija L. Castrén

Correspondence

maija.castren@helsinki.fi

In brief

Human metabolism; Neuroscience; Cell biology; Stem cells research

Gerasymchuk et al., 2026, iScience *29*, 118176
November 20, 2026 © 2026 The Author(s). Published by Elsevier Inc.
https://doi.org/10.1016/j.isci.2026.118176

CellPress

iScience

CellPress
OPEN ACCESS

Article

Astrocytes contribute to long-chain polyunsaturated fatty acid metabolism affecting microglia in fragile X syndrome

Dmytro Gerasymchuk,[1,2,10] Karo Talvio,[1,10] Andrew H. House,[3,4] Dimitri Meistermann,[4,5] Alexey S. Pospelov,[4,6] Ilari Kousa,[1,3,4] Hanna Ruhanen,[3,4] Marja Koskuvi,[6] Jere Paavola,[7,8] Minna Holopainen,[3,4] Iryna M. Ethell,[9] Jari Koistinaho,[2,6] Reijo Käkelä,[3,4] and Maija L. Castrén[1,11,*]

[1]Department of Physiology, Faculty of Medicine, University of Helsinki, 00014 Helsinki, Finland
[2]Division of Pharmacology and Pharmacotherapy, Faculty of Pharmacy, University of Helsinki, 00014 Helsinki, Finland
[3]Helsinki University Lipidomics Unit, HiLIPID, Helsinki Institute of Life Science, HiLIFE, Biocenter Finland, University of Helsinki, Biocenter 3, 00014 Helsinki, Finland
[4]Department of Molecular and Integrative Biosciences, Faculty of Biological and Environmental Sciences, University of Helsinki, Helsinki, Finland
[5]Institute of Biotechnology, Helsinki Institute of Life Science, University of Helsinki, 00014 Helsinki, Finland
[6]Neuroscience Center, Helsinki Institute of Life Science, University of Helsinki, Helsinki, Finland
[7]Minerva Foundation Institute for Medical Research, Helsinki, Finland
[8]Heart and Lung Center, University of Helsinki and Helsinki University Hospital, Helsinki, Finland
[9]Division of Biomedical Sciences, University of California, Riverside, School of Medicine, Riverside, CA, USA
[10]These authors contributed equally
[11]Lead contact
*Correspondence: maija.castren@helsinki.fi
https://doi.org/10.1016/j.isci.2026.118176

SUMMARY

Polyunsaturated fatty acids (PUFAs) influence membrane structure and function, energy metabolism, inflammation, and the ability to regulate microglial activity. We show involvement of astrocytes in long-chain PUFA metabolism in human induced pluripotent stem cell (hiPSC)-derived astrocytes with fragile X syndrome (FXS). FXS astrocytes secreted more n-6 docosapentaenoic acid (n-6 DPA) and displayed a higher n-3 DPA to docosahexaenoic acid (DHA) ratio in medium than controls, consistent with an altered n-6 to n-3 PUFA balance in plasma from the FXS mouse. The FXS-specific increase in n-6 DPA secretion was abolished by treatment with all-*trans* retinoic acid (ATRA), which affected gene expression in astrocyte subpopulations and modulated secreted triacylglycerol species. Microglial exposure to n-6 DPA stimulated expression of brain-derived neurotrophic factor (*BDNF*), which also tended to increase in microglia with reduced inflammatory marker expression when cultured in medium from ATRA-treated astrocytes. The results indicate that astrocyte-mediated n-6 DPA regulates the trophic functions of microglia in FXS.

INTRODUCTION

Fragile X syndrome (FXS) is a clinically well-characterized neurodevelopmental disorder which represents the most common monogenic cause of autism.[1] Although FXS is considered a rare disease, with an estimated prevalence of around 1 in 7,000 males and 11,000 females, its lifelong manifestation significantly amplifies its relevance. The cognitive impairment seen in FXS can range from mild to severe, and it is combined with varying degrees of autistic behaviors, hyperactivity, anxiety, and epilepsy.[2]

The molecular pathology of FXS is primarily attributed to the defective transcription of the *FMR1* gene due to a CGG trinucleotide repeat expansion in the 5′ untranslated region.[3] The absence of FMR1 protein (FMRP) disrupts synaptic function by impairing the regulation of mRNA translation at synapses, a critical process for synaptic plasticity and neuronal communication.[4] FMRP is known to interact with many mRNAs that encode proteins crucial for neuronal development and synaptic function.[5] The expression of FMRP in astroglia during synaptogenesis suggests that astrocytes contribute to the pathophysiology of FXS.[6] The absence of FMRP in astrocytes has been shown to result in aberrant secretion profiles,[7] which can affect neuronal development and synaptic refinement.

Astrocytes comprise a significant cell population in the brain, and their functional alterations have been identified in several neurodevelopmental diseases.[8] Astrocytes contribute to the control of neuronal activity, release of neurotransmitters, and processes of synaptic pruning that shape neural circuits and affect behavior.[9] Astrocytes maintain brain homeostasis and support neuronal metabolism.[10] Lipid metabolism in astrocytes allows

This is an open access article under the CC BY license (http://creativecommons.org/licenses/by/4.0/).

the brain to optimally utilize fatty acids (FAs) that are channeled into synthesis of membrane phospholipids or storage in triacylglycerols (TGs), a primary energy source for cells.[11] Astrocytes take up essential polyunsaturated FA (PUFA) precursors and express enzymes required for their conversion through consecutive elongations and desaturations to long-chain PUFAs (LC-PUFAs) with 20 or more carbon atoms, most of which are released for neurons.[12] PUFAs determine membrane fluidity, microdomain organization, and functional properties of the integral proteins in neuronal cells.[13,14]

The essential PUFAs are categorized into the n-3 and n-6 families, distinguished by the position of their first double bond at either the third or sixth carbon, respectively, when counted from the terminal methyl group.[15] In astrocytes, the nutritionally essential 18-carbon precursors of both families, alpha-linolenic acid (ALA, 18:3n-3) and linoleic acid (LA, 18:2n-6), are converted to 20- and 22-carbon LC-PUFAs with 4 to 6 double bonds. These pathways involve alternating activities of desaturases Δ-6D and Δ-5D, encoded by the *FADS2* and *FADS1* genes, respectively, to insert double bonds, and elongases (ELOVL5 and ELOVL2) that add 2-carbon units to the carboxyl terminus of the chain. To produce the end products docosahexaenoic acid (DHA, 22:6n-3) and n-6 docosapentaenoic acid (n-6 DPA, 22:5n-6) via 24-carbon intermediates, the pathway requires a third elongation (ELOVL2) and a second Δ-6D-mediated desaturation step followed by transfer to the peroxisome for a final partial β-oxidation.[12] Within the n-3 family, the DHA, n-3 docosapentaenoic acid (n-3 DPA, 22:5n-3), and eicosapentaenoic acid (EPA, 20:5n-3) are considered central to neural functions. Cellular functions also require n-6 PUFAs, particularly arachidonic acid (AA, 20:4n-6), but excess AA poses a threat of chronic inflammation. However, the signaling roles of n-6 DPA (22:5n-6), synthesized by the same enzymes as DHA and thus serving as its counterpart, are still poorly understood. Elevated tissue levels of n-6 DPA have been interpreted as indicative of impaired DHA availability.[16–18] Both n-3 and n-6 PUFAs are crucial for brain development, and as biologically distinct compounds, may possess complementary as well as unique functional roles.[19] Insufficient dietary intake and resulting low tissue levels of n-3 PUFAs have been implicated in heightened susceptibility to various neuropsychiatric disorders.[15] FXS individuals are shown to exhibit reduced plasma levels of FAs, particularly n-3 PUFAs,[20] and similar PUFA alterations are observed in children with autism.[21] Studies conducted on murine models of FXS have demonstrated that supplementation with n-3 PUFAs can yield beneficial effects on the behavioral phenotype and neuroinflammatory responses.[22–24]

We investigated PUFA metabolism in FXS forebrain astrocytes, derived from human induced pluripotent stem cells (hiPSCs), and found elevated n-6 DPA levels in FXS astrocyte-conditioned medium (ACM) compared with controls. In addition, an elevated n-3 DPA to DHA ratio in FXS astrocytes indicated defective n-3 PUFA metabolism. Single-cell RNA sequencing (scRNA-seq) defined functional subpopulations of astrocytes with FXS-related changes in expression of genes involved in metabolism of lipids, especially of LC-PUFAs. In plasma from an FXS mouse model, *Fmr1* knockout (KO) mice, the altered PUFA balance was associated with an increased palmitate (PA, 16:0) level that can influence retinoic acid (RA) signaling by favoring its conversion to storage as retinyl PA. The enhanced release of n-6 DPA from FXS cells was diminished when the cells were treated with all-*trans* RA (ATRA), and simultaneously, the elevated intracellular calcium (Ca^{2+}) responses to ATP were normalized. Treatment with n-6 DPA increased microglial *BDNF* mRNA expression in a dose-dependent manner. Additionally, ACM from ATRA-treated astrocytes showed a tendency to increase *BDNF* expression and reduce microglial expression of pro-inflammatory cytokines. These findings highlight elevated n-6 DPA levels in FXS ACM as an indicator of altered astrocytic PUFA balance, which modulates neurotrophic and inflammatory properties of microglia regulating neuronal functions in FXS.

RESULTS

FA alterations in *Fmr1* KO mouse plasma

FMRP is involved in the control of lipid metabolism, and the amounts of circulating free and total FAs are shown to be altered in human and mouse FXS blood.[20,25] We examined the FA composition in *Fmr1* KO mouse plasma using gas chromatography with mass spectrometric detection (GC-MSD) and gas chromatography with flame ionization detection (GC-FID). We observed that the PUFA levels were lower, while the saturated FA (SFA) levels (mol%) were higher in the *Fmr1* KO plasma compared with wild type (Figure 1A). The plasma FA changes were identical in male and female *Fmr1* KO mice (Figure S1). The ratio of n-6 DPA to AA was increased in the *Fmr1* KO plasma (Figure 1B), suggesting altered LC-PUFA processing in FXS. Additionally, the ratio of n-6 DPA to DHA was increased in the *Fmr1* KO plasma (Figure 1C), indicating a preference for the n-6 over the n-3 PUFA pathways in FXS. Elevated SFA level in *Fmr1* KO plasma resulted especially from an increase in PA that promotes insulin resistance and inflammation unlike the protective n-3 PUFAs such as DHA[26] (Figure 1D).

Increased n-6 PUFAs in hiPSC-derived FXS astrocyte secretome

To investigate putative defects in PUFA metabolism in the FXS brain, we studied human FXS astrocytes, focusing on their crucial role in maintaining brain lipid homeostasis and coordinating immune responses.[27] A previously described set of FXS and control hiPSC lines was used to generate human FXS and control forebrain astrocytes, the hASTRO model.[28] Our method of astrocyte differentiation specifies neural progenitors into astrocytes using ciliary neurotrophic factor (CNTF), providing cells with neurosupportive properties (Figure 2A).[29] Cells cultured >90 days *in vitro* (DIV) acquired astrocytic morphology and expressed astrocytic markers (Figure 2B). Transcriptomic analysis of differentiating astrocytes[30] showed increased expression of vimentin and CD44 during differentiation into hASTRO, indicating amplified reactivity[31] in both FXS and control astrocytes. However, the expression levels of a set of reactivity markers did not differ between FXS and control astrocytes at 95 DIV under basal culturing conditions (Figure 2C).

We compared the long-chain free fatty acid (FFA) levels in ACM from FXS and control astrocytes using liquid chromatography-tandem mass spectrometry (LC-MS/MS) to

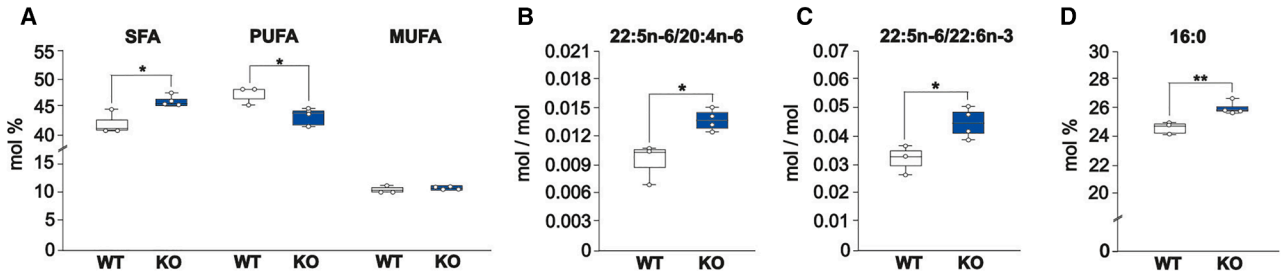


Figure 1. Fatty acids in plasma from *Fmr1* knockout and wild-type male mice

(A) Saturated (SFA), polyunsaturated (PUFA), and monounsaturated (MUFA) fatty acid content in plasma from wild-type (WT) and *Fmr1* KO mice.

(B and C) The ratio of 22:5n-6 (n-6 docosapentaenoic acid, DPA) to 20:4n-6 (arachidonic acid, AA), (C) the ratio of n-6 DPA to 22:6n-3 (docosahexaenoic acid, DHA), and (D) the levels of palmitic acid (16:0) in WT and *Fmr1* KO plasma. *n* (WT) = 3 and *n* (*Fmr1* KO) = 4 mice.

Data are shown as mean ± SEM. The two-tailed unpaired *t* test was applied to evaluate the statistical significance between the WT and *Fmr1* KO samples. Statistical significance is defined as follows: $^{*}p < 0.05$ and $^{**}p < 0.001$.

identify FXS-specific differences in PUFA metabolism. The levels of essential n-6 and n-3 PUFA precursors LA and ALA, respectively, were similarly lower in FXS and control ACM compared with the levels in the medium without cells, indicating the uptake of LA and ALA by astrocytes (Figure 2D). Also, PA and stearic acid (18:0) were identically reduced in FXS and control ACM (Figure 2D). The levels of several LC-PUFAs, such as EPA, n-3 DPA, AA, n-6 DPA, and saturated arachidic acid (20:0) were higher in ACM from both control and FXS cells than in media without cells (Figure 2E), indicating that these FAs were released from astrocytes. The n-6 DPA levels were much higher in FXS ACM than in control ACM (Figure 2F). A concomitant increase in n-3 DPA did not reach the level of significance, but the ratio of n-3 DPA to DHA (22:5n-3/22:6n-3) was increased in three FXS biological replicates, indicative of a defective n-3 pathway (Figure 2G). In addition, erucic acid (22:1n-9) content was smaller in control ACM than in FXS ACM or the medium without cells (Figure 2E), suggesting a slight decrease in the uptake of 22:1n-9 into FXS astrocytes compared with controls.

Since hydrolysis of TGs and phospholipids generates FFAs, we investigated potential TG changes associated with the increased n-6 DPA in FXS ACM. We observed that the levels of TGs containing SFAs showed a tendency to be lower and those containing PUFAs higher in FXS ACM compared with controls (Figure 2H). Highly varying concentrations of unsaturated TG species (TG52:3, TG52:4, TG54:4, TG54:5, and TG54:6) in FXS ACM likely reflected their contribution to the regulation of the cellular PUFA content through transport (Figure 2H). As an exception, TGs containing long-chain SFAs were especially abundant in ACM from the HEL100.2 FXS cell line derived from an FXS donor with epilepsy. The transcriptomic analysis of neural progenitors generated from this cell line displayed pronounced epilepsy-related features when compared with the progenitors derived from the other FXS cell lines.[32]

Lipid differences in human FXS and control astrocytes

Although the lipid class compositions of FXS and control hiPSC-derived astrocytes were comparable, as illustrated in Figure 3A, analysis of their individual lipid species profiles revealed distinct segregation when subjected to principal component analysis (PCA, Figure 3B). In FXS astrocytes, the profile of TG species was skewed toward species with two to five double bonds, reflecting uptake and incorporation of LA and ALA, which contain two and three double bonds, respectively. In contrast, control astrocytes exhibited a higher presence of species containing SFAs but also some highly unsaturated species, as depicted in Figure 3C. Statistical analysis revealed that the TG species 52:3 had significantly greater mol% values in FXS astrocytes, whereas the TG species 48:1 and 52:5 were more prevalent in the control group (Figure 3D).

Astrocyte subpopulations expressing genes involved in PUFA metabolism

To examine whether the increase in n-6 PUFA release from FXS astrocytes was associated with functional subpopulations, we performed scRNA-seq of control (PO2) and FXS astrocytes (HEL69.5 and HEL100.1). Clustering analysis identified 10 functional clusters of astrocytes hallmarked by specific transcription factor expression (Figure 4A). To refine the characterization of these clusters, we computed gene modules that we named with a representative transcription factor (see STAR Methods) and added a level of annotation to the cells, grouping cell clusters into superclusters. FXS and control astrocytes showed considerable differences in the cell population analysis (Figures 4A–4C). The cycling supercluster was identified by the expression of the transcription factor *SOX2* (SOX2.mod). Astrocytes in this cluster particularly expressed genes that play critical roles in various signaling pathways that ensure proper cell division and genomic stability (*CDK1*, *TOP2A*, *CENPF*, *KIF11*, *TUBA1B*, *NUSAP1*, and *CENPF*). Furthermore, the cluster expressed genes involved in lipid biosynthesis, especially in the desaturation and elongation of PUFAs (*FADS1* and *ELOVL5*).[33] The SOX2 cluster was more prominent in HEL69.5 hiPSC-derived FXS astrocytes than in astrocytes derived from other cell lines (Figure 4C), in agreement with augmented SOX2 expression observed previously in FXS neural progenitors.[34,35] The ImmunoDev supercluster was marked by the PAX3 module (PAX3.mod) and contains genes related to both neuronal development (*NTRK2*, *DCLK1*, *CDH6*, and *TENM2*) and antigen presentation/immunity (*IFITM1*, *HLA-B*, *A2M*, and *CLU*). The two clusters related to the ImmunoDev supercluster (specifically, cluster ImmunoDev.matureAstro and ImmunoDev.immature)

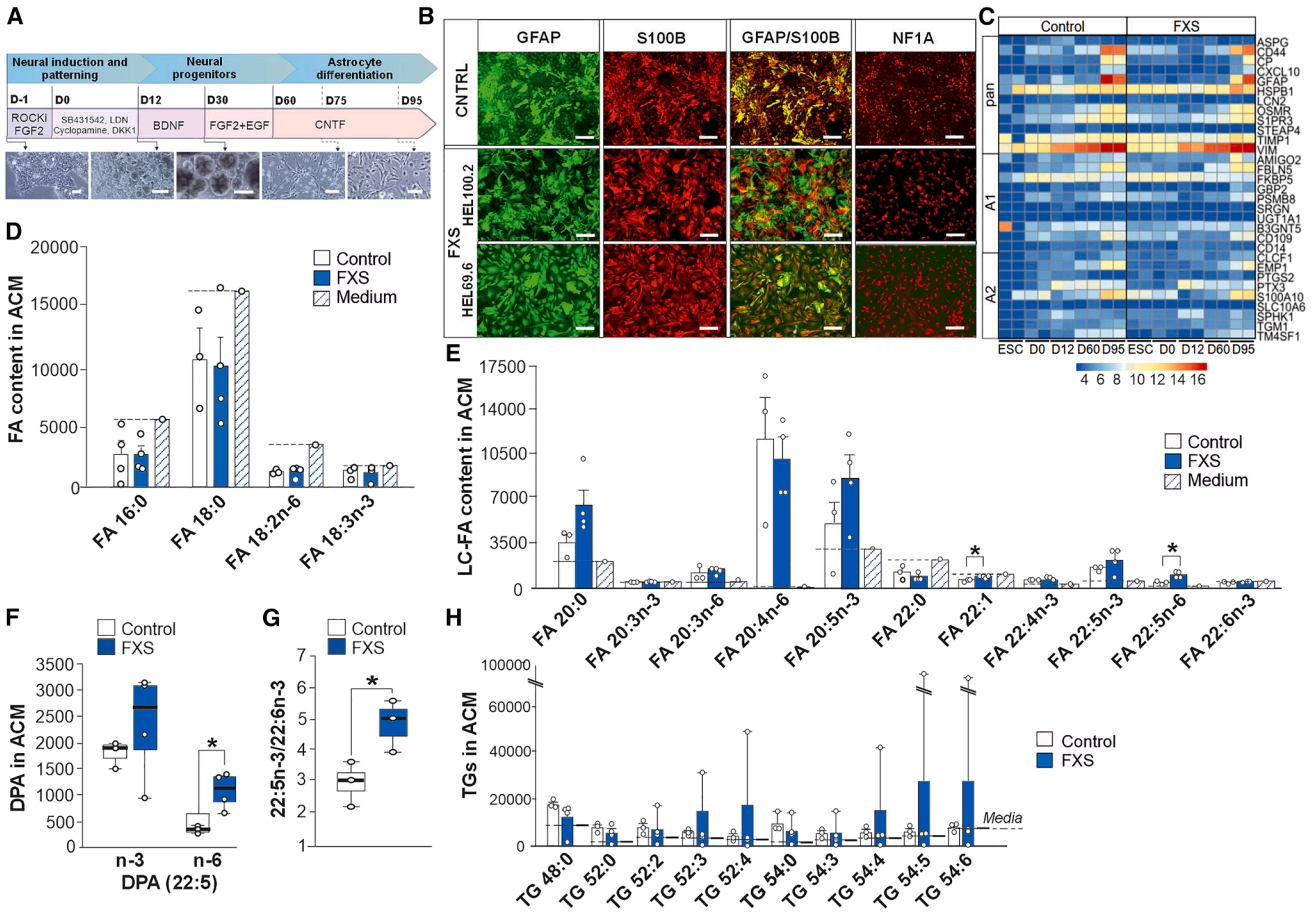


Figure 2. Human forebrain astrocytes derived from FXS and control pluripotent stem cells and content of fatty acids and triacylglycerol species in ACM

(A) Schematic presentation of the hiPSC-derived astrocyte differentiation method.

(B) Expression of astrocyte markers GFAP, S100B (green and red, respectively, and an overlay) and NF1A (red) in human astrocytes derived from a control and two FXS (HEL69.6 and HEL100.2) hiPSC lines.

(C) Heatmap showing expression of reactivity markers in bulk RNA-seq analysis of cells derived from the isogenic human embryonic stem cell (ESC)-derived FXS and control cell lines on days 0, 12, 60, and 95 during differentiation of astrocytes.

(D) Reduced levels of palmitic acid (FA16:0), stearic acid (FA18:0), linoleic acid (FA18:2), and alpha-linolenic acid (FA18:3) in control and FXS ACM.

(E) Levels of long-chain fatty acids (LC-FAs) in control and FXS ACM.

(F) n-3 and n-6 DPA in control and FXS ACM.

(G) The ratio of n-3 DPA/DHA (22:5n-3/22:6n-6) in control and FXS ACM.

(H) Triacylglycerol (TG) species in control and FXS ACM.

N (control) = 3 cell lines and *N* (FXS) = 4 cell lines (3 biologically independent cell lines) (D–H). FA and TG contents are shown as mean intensity of mass spectrometric signal, and data are shown as mean ± SEM. The two-tailed unpaired *t* test was applied to evaluate the statistical significance between the FXS and control samples (D–H). Scale bars, 50 μM (A), 100 μM (B). *$p < 0.05$.

mainly differed in terms of maturity markers. Notably, the ImmunoDev.immature cluster was strongly enriched in HEL100 FXS cells (Figure 4C). The morph supercluster was characterized by enrichment of the *TCF12* gene module (TCF12.mod). Genes enriched in this supercluster were associated with diverse astrocyte functions, ranging from basic cellular processes such as metabolism and adhesion to more complex functions including signaling and responses to external stimuli (*NES*, *TEAD1*, *NFAT5*, *TCF12*, *STAT3*, *DLG1*, and *VLC*). Especially, the enriched genes belonged to the epithelial-mesenchymal transition-related pathways (*TGFB2*, *IGF1R*, and *IGFBP3*), WNT signaling (*TCF4* and *TEAD1*) and cytoskeleton reorganization (*SEMA6A* and *DNM3*). The cluster Morph.FXS.neurogen of FXS astrocytes was larger than that of control astrocytes and expressed *FADS2*, which is needed for LC-PUFA desaturation (Figure 4D). The HES6 supercluster (Hes6.mod) contained many genes whose functions are related to cellular and tissue structural integrity, such as cytoskeletal organization and extracellular matrix stability (*THBS1*, *ANKRD1*, *MFAP5*, *MYL9*, *IGFBP3*, and *GAS6*), as well as signaling pathways that regulate cellular growth, differentiation, and survival (*ACTG2* and *PLD5*). The MetaboHigh supercluster was defined by the *JUND* gene

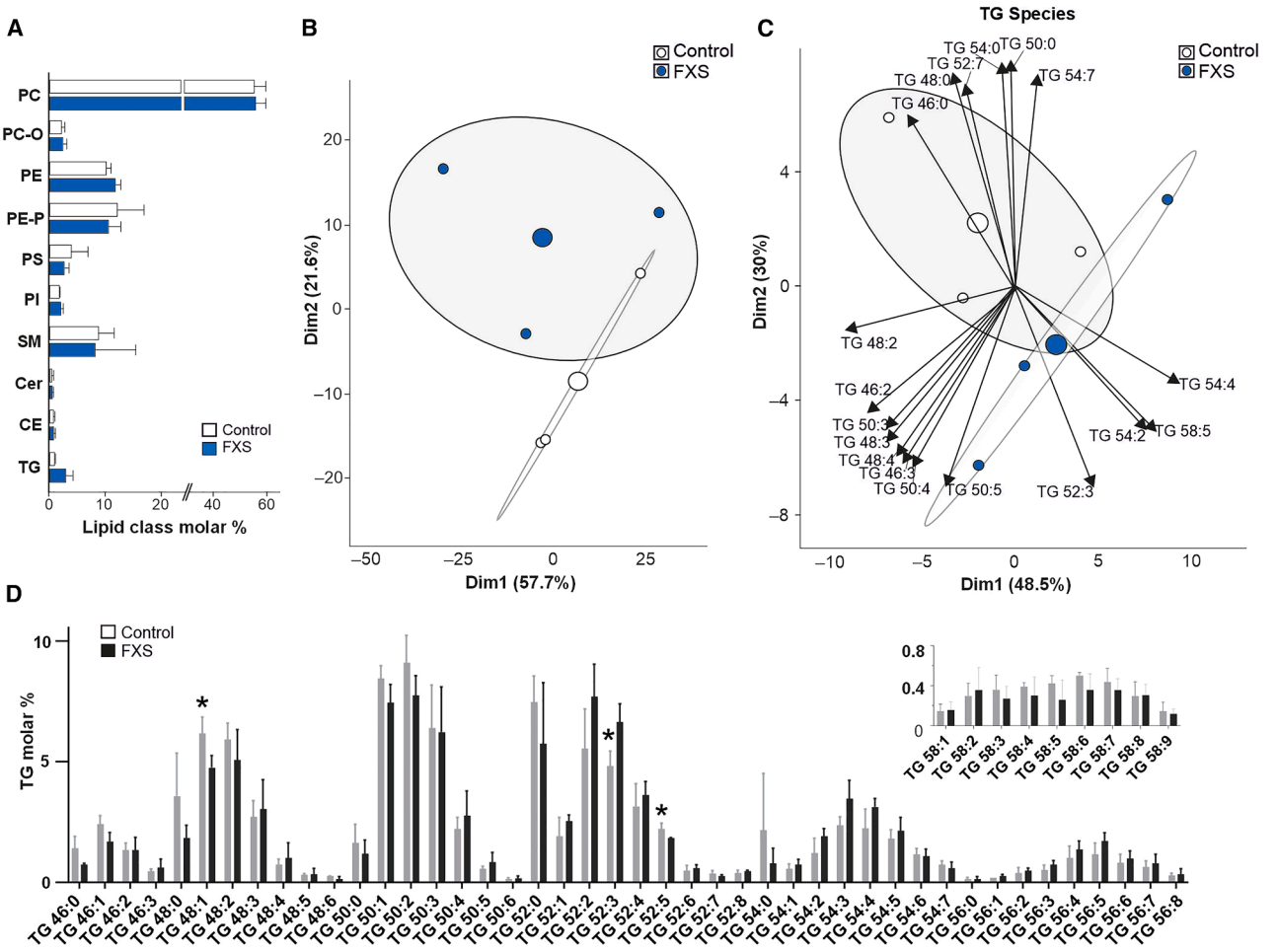


Figure 3. Comparison of the lipidome between FXS and control human forebrain astrocytes

(A) Proportions of different lipid classes in FXS (HEL69.6, HEL70.6, and HEL100.2) and control (HEL23.3, HEL24.4, and PO2) hiPSC-derived astrocytes.

(B) Principal component analysis using as loadings 212 detected lipid species (53 TG, 14 CE, 6 Cer, 6 SM, 15 PI, 26 PS, 16 PE P, 34 PE, 16 PC O, and 26 PC species) normalized to their respective lipid class in three biological replicates of male FXS (HEL69.6, HEL70.6, and HEL100.2) and control (HEL23.3, HEL24.4, and PO2) astrocytes.

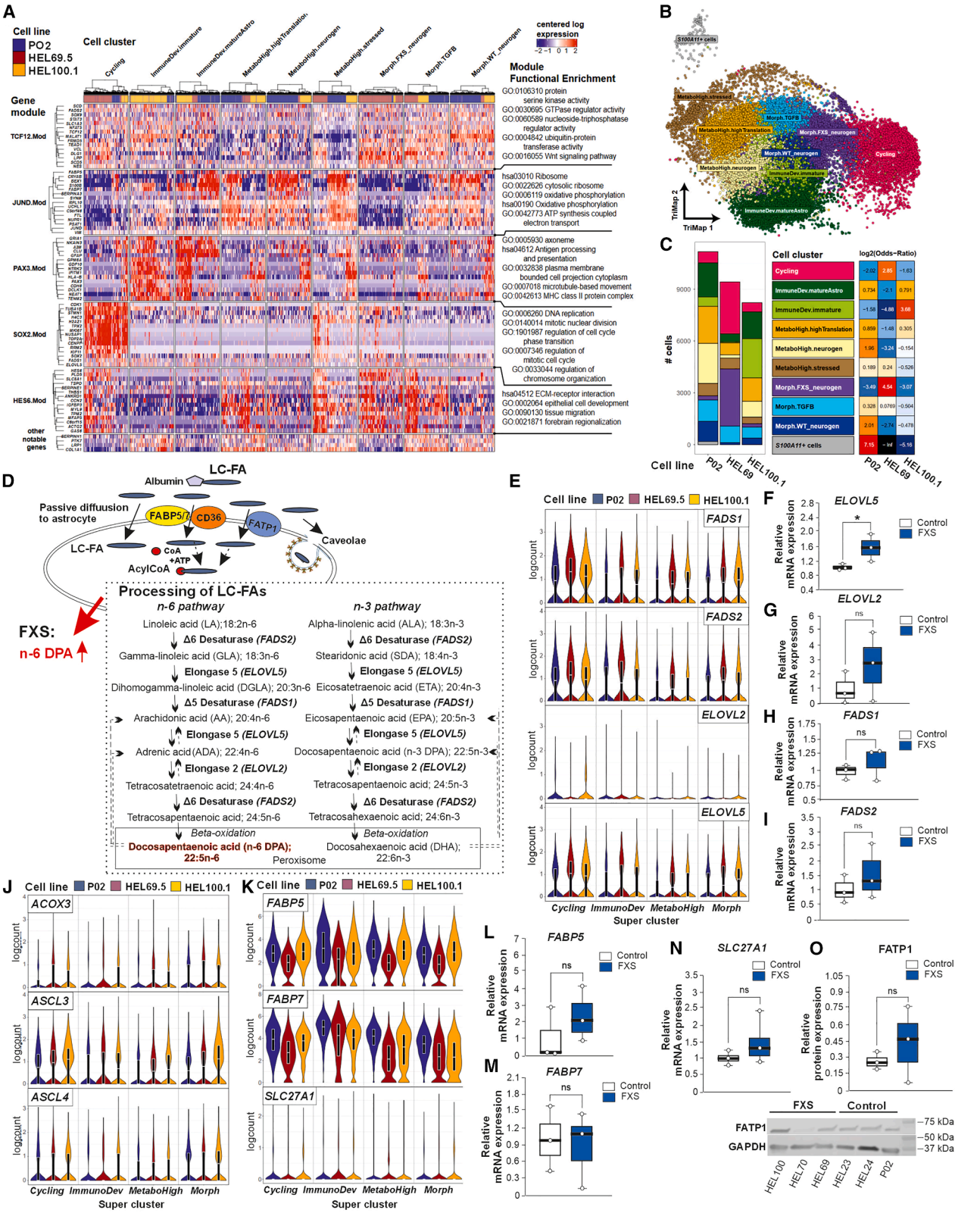
(C) Principal component analysis of FXS (HEL69.6, HEL70.6, and HEL100.2) and control (HEL23.3, HEL24.4, and PO2) astrocytes using the loadings detected 53 TG species and showing the top 18 species in the biplot.

(D) TG mol% profile of FXS and control astrocytes. The TG species are named according to [sum of carbons]:[sum of double bonds] in the three acyl chains. Data are presented as mean ± SEM. The two-tailed unpaired *t* test was applied to evaluate the statistical significance between the FXS and control samples. *$p < 0.05$. TG, triacylglycerol; CE, cholesteryl ester; Cer, ceramide; SM, sphingomyelin; PI, phosphatidylinositol; PS, phosphatidylserine; PE P, alkenyl-acyl phosphatidylethanolamine; PE, diacyl phosphatidylethanolamine; PC O, ether species of phosphatidylcholine (largely alkyl-acyl species); PC, diacyl phosphatidylcholine.

module (JUND.mod) and exhibited a highly metabolic and reactive astroglial profile. Transcripts enriched in this cluster are involved in protein synthesis and folding (*RPL* and *RPS* series, *EEF1A1*, *RACK1*, and *CRYAB*), amino acid and nutrient metabolism (*PSAT1*, *MTHFD2*, *SLC3A2*, *FABP5*, and *FABP7*), and oxidative damage prevention, including maintenance of iron and calcium homeostasis (*GPX1*, *SELENOW*, *FTH1*, *FTL*, *CRYAB*, *FTH1*, and *S100B*).

Expression of genes required in LC-PUFA elongation and desaturation (Figure 4D) was particularly enriched in cycling and morph superclusters with lower expression levels in the other clusters (Figure 4E). Using quantitative reverse-transcription polymerase chain reaction (RT-qPCR) to analyze astrocytes derived from three FXS and three control hiPSC lines, an elevated *ELOVL5* expression in FXS astrocytes was found (Figures 4E and 4F), also suggesting altered PUFA elongation in FXS. Expression of *ELOVL2*, *FADS1*, and *FADS2* did not differ between FXS and control astrocytes (Figures 4E and 4G–4I). Genes involved in lipid metabolism (based on Gene Ontology) were expressed across all superclusters, including *ACOX3* and *ACSL4*/*ACSL3*, which are involved in peroxisomal FA β-oxidation and activation of FFAs, respectively (Figure 4J).

Next, we explored the potential contribution of FA transporters to FXS-specific astrocytic PUFA changes (Figure 4D). The



(legend on next page)

FA-binding proteins *FABP5* and *FABP7* were expressed across all superclusters (Figure 4K), and their expression levels did not differ between FXS and control astrocytes (Figures 4L and 4M). FATP1 is an insulin-sensitive FA transporter with high affinity for long and very long-chain FAs, including PA and PUFAs, and it also exhibits acyl-CoA synthetase activity.[36] Expression of the *SLC27A1* gene encoding FATP1 was low and did not differ between FXS and control astrocytes (Figures 4K and 4N), as observed previously in embryonic stem cell (ESC)-derived FXS astrocytes compared with isogenic controls.[30] Furthermore, FATP1 protein expression showed substantial cell line-dependent variation, and mRNA levels did not correlate with protein expression (Figure 4O). This may indicate the activation of individual cell line-dependent transcriptional and post-transcriptional mechanisms that regulate astrocytic FA acid uptake and processing.

RA effect on increased n-6 DPA in FXS ACM

Since RA supplementation affects social behavior in *Fmr1* KO mice similarly to n-3 PUFA supplementation,[22,37] and PUFAs can act as natural ligands for the RA receptor (RXR),[38] we investigated the effects of RA treatment on astrocytes and n-6 DPA in FXS ACM. ATRA has been previously shown to reduce the PUFA n-6/n-3 ratio in mammary epithelial cells.[39] We found that treatment of astrocytes with 10 μM ATRA for 24 h prevented the increase in n-6 DPA (Figure 5A), without affecting n-3 DPA levels (Figure 5B) or reducing the ratio of n-6 DPA/DHA in FXS ACM (Figure 5C). ATRA also reduced the variability of total TG in FXS ACM by lowering the levels of TG species containing LC-PUFAs (Figure 5D). In HEL100.2 ACM, the proportion of TGs containing SFAs was increased in response to ATRA treatment (Figure 5E) compared with other FXS ACM samples, supporting donor-dependent differences in FA metabolism in astrocytes derived from the HEL100 FXS cell lines. ATRA did not affect cell survival at the concentration used (Figure 5F).

ATRA treatment abolished the difference in *ELOVL5* expression between FXS and control astrocytes by increasing the variability in FXS cells (Figure 5G), which may reflect differences in the RA-related mechanisms regulating PUFA balance in astrocytes derived from different FXS cell lines. FABP5 and FABP7 are tightly linked to the regulation of RA signaling,[40,41] and astrocytic *FABP7* tended to decrease after ATRA treatment, but *FABP5* and *FABP7* expression levels did not differ between FXS and control astrocytes (Figures 5H and 5I). It is noteworthy, however, that the expression of *SLC27A1* coding for FATP1 was reduced (75% of control) in FXS astrocytes after ATRA treatment, while ATRA did not reduce the *SLC27A1* expression levels in control astrocytes (127% of control) (Figure 5J).

Effects of ATRA on intracellular Ca^{2+} responses in FXS astrocytes

Differences in membrane PUFA content modulate the packing and microdomain organization of the membrane, having an impact on activation of G-protein-coupled membrane receptors and store-operated calcium influx.[42] Since n-6 and n-3 PUFAs may exert differential effects on calcium signaling pathways,[43] we examined whether the increased release of n-6 DPA was associated with altered intracellular calcium ($[Ca^{2+}]_i$) dynamics in FXS astrocytes. To this end, we measured ATP-induced elevations of $[Ca^{2+}]_i$ resulting from the activation of Gq-coupled purinergic receptors[44] using Fura-2-based ratiometric fluorescence recordings. The ATP-induced increase in $[Ca^{2+}]_i$ showed substantial variability in both control and FXS astrocytes, reflecting functionally heterogeneous astrocyte subpopulations (Figures 5K and 5L). The average $[Ca^{2+}]_i$ was larger ($p < 0.001$) in FXS astrocytes than in controls (Figure 5L). Exposure to ATRA normalized the $[Ca^{2+}]_i$ response in FXS astrocytes (Figure 5M), which may reflect changes in cell membrane structure associated with altered PUFA balance.

Effects of n-6 DPA on microglia

Inflammatory responses of FXS microglia have been shown to be abnormal,[45] and increased secretion of n-6 DPA from FXS astrocytes may contribute to extrinsic mechanisms underlying defective microglial pruning of neuronal synapses in FXS.[46] There is evidence that n-3 DPA protects neurons from neuroinflammation-induced damage by modulating microglial M1/M2 polarization through a BDNF-mediated mechanism.[47] However, n-6 and n-3 PUFAs may exert opposite effects in inflammation-related processes.[48] We found that n-6 DPA increased *BDNF* expression in hiPSC-derived microglia in a dose-dependent manner (Figure 6A). Treatment with n-6 DPA did not have any significant effects on the microglial tumor necrosis factor (*TNF*)

Figure 4. Expression of genes involved in fatty acid metabolism in control and FXS astrocytes and their functional subtypes

(A) Heatmap of the expression profile of the gene modules identified in human forebrain astrocytes derived from control (PO2) and FXS (HEL69.5 and HEL100.1) hiPSC lines. Altogether, 500 cells were drawn from each astrocyte cell cluster. A selection of 15 representative genes is shown for each gene module, with an additional set of genes not belonging to any selected module (see STAR Methods). A representative set of terms retrieved by functional enrichment is indicated on the right.

(B) TriMap 2D embedding of the scRNA-seq dataset, colored by cell cluster.

(C) Barplot of abundance of cell clusters per cell line (left), completed by the association value as log2(odds ratio [OR]) between cell clusters and cell lines (right).

(D) Schematic representation of n-6 and n-3 PUFA metabolism.

(E) Gene expression of *FADS1*, *FADS2*, *ELOVL2*, and *ELOVL5* in the control (PO2) and FXS (HEL69.5 and HEL100.1) cell lines by supercluster, using violin and boxplots.

(F–I) Expression of (F) *ELOVL5*, (G) *ELOVL2*, (H) *FADS1*, and (I) *FADS2* in FXS and control human astrocytes. *N* (control) = 3 and *N* (FXS) = 3 cell lines, representing biological replicates.

(J and K) (J) Gene expression of *ASCOX3*, *ASCL3*, and *ASCL4*, and (K) expression of *FABP7*, *FABP5*, and *SLC27A1* in the control (PO2) and FXS (HEL69.5 and HEL100.1) cell lines by supercluster, using violin and boxplots.

(L–N) Expression of (L) *FABP7*, (M) *FABP5*, and (N) *SLC27A1* in FXS and control astrocytes. *N* (control) = 3 and *N* (FXS) = 3 cell lines, representing biological replicates.

(O) FATP1 protein in control and FXS astrocytes in western blot analysis.

Data are shown as mean ± SEM. A two-tailed unpaired *t* test was applied to evaluate the statistical differences. $^*p < 0.05$.

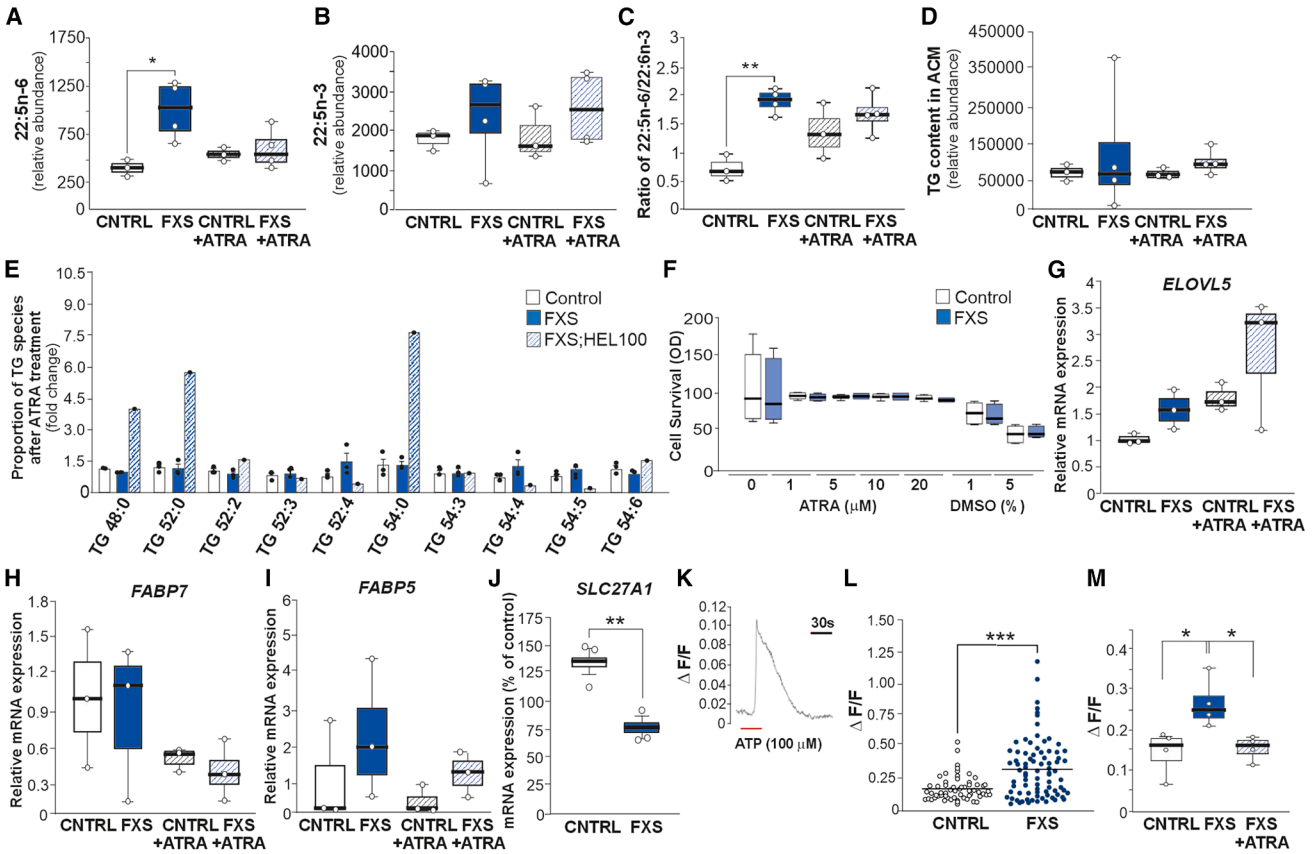


Figure 5. Effects of ATRA treatment on FXS and control ACM, astrocytic fatty acid transporter expression, and Ca^{2+} signaling

(A–D) (A) n-6 DPA (22:5n-6), (B) n-3 DPA (22:5n-3), (C) the ratio of n-6 DPA to DHA (22:5n-6/22:6n-3), and (D) triacylglycerol (TG) content in FXS and control (CNTRL) ACM without and with ATRA treatment (10 μM) for 24 h. *N* (CNTRL) = 3 cell lines; *N* (FXS) = 4 cell lines (3 biologically independent cell lines).

(E) Proportions of TG species per total TGs in ACM from three control and three FXS iPSC clones derived from donors without epilepsy compared to those in ACM from astrocytes derived from an FXS donor with epilepsy (FXS; HEL100).

(F) Cell survival after treatment with different concentrations of ATRA and DMSO. The assay was performed with five control and four FXS replicates.

(G–J) Expression of (G) *ELOVL5*, (H) *FABP7*, and (I) *FABP5* in untreated and ATRA-treated CNTRL and FXS astrocytes. (J) Changes in the expression of *SLC27A1* (% of CNTRL) after ATRA treatment in CNTRL and FXS astrocytes. In (G)–(J), *N* (CNTRL) = 3 and *N* (FXS) = 4 (3 biologically independent cell lines) in both untreated and ATRA-treated experimental groups.

(K) Representative single-cell $[Ca^{2+}]_i$ response to ATP in hiPSC-derived astrocytes.

(L) The mean peak amplitude of $[Ca^{2+}]_i$ responses to ATP in CNTRL and FXS astrocytes. *N* (CNTRL) = 4 (84 astrocytes) and *N* (FXS) = 4 (3 biologically independent cell lines; 86 astrocytes).

(M) The $[Ca^{2+}]_i$ response in ATRA-treated FXS astrocytes compared with responses in untreated FXS and CNTRL astrocytes. Data are from 4–5 repeated experiments (>30 cells analyzed in each experiment) performed in each experimental group.

Data are shown as mean ± SEM. One-way ANOVA with Tukey's test for multiple comparisons and a two-tailed unpaired *t* test were applied to evaluate the statistical differences. Statistical significance is defined as follows: $^*p < 0.05$, $^{**}p < 0.01$, $^{***}p < 0.001$.

expression (Figure 6B), but it reduced interleukin-1β (*IL1B*) mRNA expression (Figure 6C). Microglia cultured with ACM from FXS or control astrocytes for 24 h expressed similar levels of the well-established microglia-specific marker Iba1, the product of the *AIF-1* gene (Figures 6D and 6E). ACM from FXS or control astrocytes did not increase *BDNF* expression to the expression level in microglia that were exposed to medium used in astrocyte cultures for 24 h. However, there was a tendency to increase microglial *BDNF* expression after exposure to ACM from astrocytes treated with ATRA (Figure 6F). Expression of pro-inflammatory surface markers *TNF* (Figure 6G) and *IL1B* (Figure 6H) did not differ in microglia cultured with FXS or control ACM. ACM collected from FXS or control astrocytes treated with ATRA reduced expression of these microglial M1 pro-inflammatory markers, consistent with the known anti-inflammatory effects of ATRA (Figures 6G and 6H). Collectively, the results suggest a role for n-6 DPA in the regulation of microglial function in FXS.

DISCUSSION

Lipids constitute approximately 50% of the brain's dry weight, with PUFAs accounting for, on average, 25% of brain FAs. Consequently, PUFA metabolism may substantially influence the onset

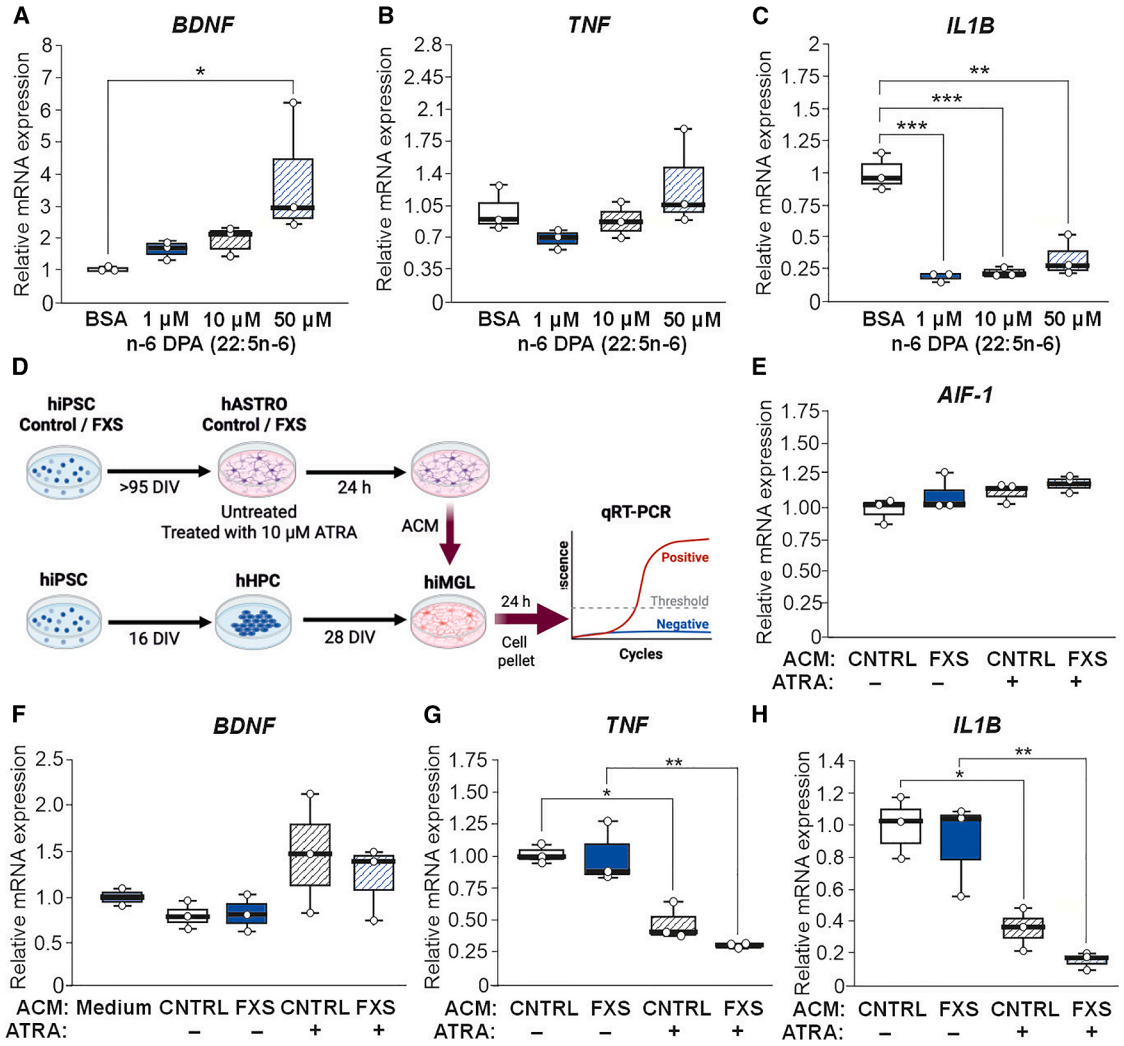


Figure 6. Effects of n-6 DPA and ACM on microglia

(A) Expression of *BDNF* mRNA in hiPSC-derived microglia treated with 1, 10, and 50 µM of n-6 DPA (22:5n-6) complexed with BSA or BSA control (50 µM).

(B and C) Microglial expression of *TNF* and *IL1B* after treatment with 1, 10, and 50 µM of n-6 DPA (22:5n-6).

(D) Schematic presentation of the study investigating effects of ACM from untreated and ATRA-treated (10 µM; 24 h) control and FXS astrocytes on hiPSC-derived microglia.

(E and F) (E) *AIF-1* and (F) *BDNF* mRNA expression in microglia cultured in astrocyte culture medium or ACM from untreated and ATRA-treated control (CNTRL) and FXS astrocytes.

(G and H) *TNF* and *IL1B* mRNA expression in microglia exposed to ACM from untreated and ATRA-treated CNTRL and FXS astrocytes. *N* (CNTRL) = 3 and *N* (FXS) = 3 biologically independent cell lines.

Data are shown as mean ± SEM. The one-way ANOVA (A–C and E–H) was used to evaluate the statistical significance between the FXS and control samples. $^{*}p < 0.05$, $^{**}p < 0.01$, $^{***}p < 0.001$.

and progression of neurological disorders. Lipids play pivotal roles in astrocyte function, particularly in intercellular communication and as structural components of cellular membranes, while also regulating inflammatory processes in the brain.[10] Astrocytes provide essential metabolic support to neurons, and lipid metabolism is central to maintaining brain homeostasis and FA-based oxidative energy metabolism.[49] Because FAs are integral components of nearly all lipid classes, their precise regulation is essential for the proper function of brain lipids.[50] Moreover, brain lipid homeostasis influences microglial function,[51] which is crucial for the development and maintenance of neuronal networks that are compromised in FXS[46] and autism.[52]

We showed elevated levels of n-6 DPA in ACM from human FXS astrocytes, reflecting altered PUFA metabolism and signaling from FXS astrocytes. As we summarize in Figure 7, astrocytic control of FA uptake and storage is associated with the dysregulation of LC-PUFA processing and elevated n-6 DPA release. ATRA treatment of FXS astrocytes reduced n-6 DPA secretion, and n-6 DPA was shown to be linked to anti-inflammatory and neurotrophic signaling in microglia.

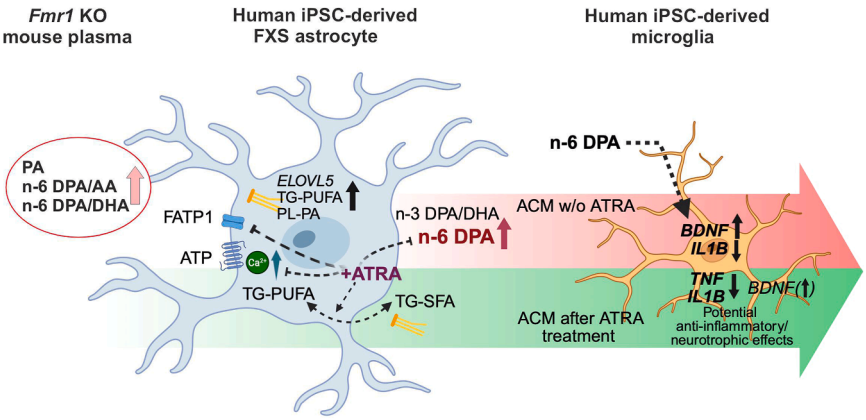


Figure 7. Graphical summary of results

Altered fatty acid metabolism and long-chain PUFA (polyunsaturated fatty acid) processing are seen as an increased ratio of n-6 DPA (docosapentaenoic acid) to AA (arachidonic acid) and to DHA (docosahexaenoic acid), along with an increase in PA (palmitic acid) levels in plasma from the FXS mouse model. Human FXS astrocytes are functionally heterogeneous, but an FXS-specific increase in n-6 DPA release and n-3 DPA to DHA ratio is associated with increases in the elongase *ELOVL5* expression needed for long-chain PUFA processing, triacylglycerols (TGs) containing PUFAs, and phospholipids with PA. ATRA (all-*trans* retinoic acid) treatment of FXS astrocytes prevents the increase in n-6 DPA release and increases PUFA content versus SFAs (saturated fatty acids) in TGs in the astrocytic secretome. These changes parallel reduced expression of the fatty acid transporter *FATP1* and the normalized intracellular calcium responses to ATP. n-6 DPA exposure increases *BDNF* expression in a dose-dependent manner. Culturing human microglia with medium from ATRA-treated astrocytes leads to reduced microglial inflammatory marker expression and a tendency toward increased *BDNF* expression.

Protein transporters and passive diffusion mediate uptake of FAs into astrocytes, which deposit FAs released later to the extracellular space.[53] Brain PUFAs are mainly derived from blood, but astrocytes express genes needed for the synthesis of LC-PUFAs from the precursors.[54] Expression of elongases and desaturases required for LC-PUFA modifications was found in certain subpopulations of hiPSC-derived astrocytes in the scRNA-seq analysis. Astrocyte subpopulations showed differences between control and FXS astrocytes, with transcriptomic signatures of FXS astrocytes indicating a more immature phenotype compared to control astrocytes. This was characterized by a proliferative cell state and physiological properties such as early response to environmental cues and cell motility. Both control and FXS astrocytes showed high cell line-dependent variation in the expression of lipid transporters in functional astrocyte subtypes. These differences may contribute to the FXS phenotype variability, as suggested by the contrasting lipid profiles observed between astrocytes derived from FXS donors with and without epilepsy.

An increase in the expression of *ELOVL5*, which encodes an enzyme specialized in elongating PUFAs,[55] in FXS astrocytes compared with controls confirmed the change in PUFA metabolism in FXS astrocytes. The elevated ratio of n-6 DPA to DHA in *Fmr1* KO plasma, as well as in human FXS ACM, is consistent with the previously reported increase in the ratio of DPA to EPA in plasma phospholipids of individuals with FXS,[20] and suggests that metabolic alterations specifically drive the n-6 PUFA pathway in systemic physiology and brain. The EPA to ALA ratio (20:5/18:3) was not reduced in FXS ACM compared with controls, as previously reported in plasma phospholipids from FXS patients, in agreement with the capacity of astrocytes to produce LC-PUFAs.[12] Because disturbances in n-3 PUFA metabolism can lead to excessive elongation and desaturation of n-6 PUFAs,[16–18] the increased n-6 DPA observed in FXS ACM may represent a compensatory response to impaired n-3 PUFA metabolism. Supporting this possibility, studies using *Fmr1* KO rodent models have shown that perinatal supplementation with n-3 PUFAs can attenuate hyperactivity and improve learning as well as social behavior in the *Fmr1* KO phenotype.[22–24] Interestingly, these beneficial effects differ from those observed with post-weaning supplementation, which has been reported to reduce startle responses but impair freezing behavior during fear conditioning, indicating an inhibited learning of the acquired response.[24] An elevated ratio of n-6 to n-3 PUFA has also been observed in the blood of patients with attention deficit hyperactivity disorder (ADHD)[56] and autism,[21] both of which are frequently comorbid with FXS.[2] Clinical studies investigating n-3 PUFA supplementation in individuals with autism have provided evidence of beneficial effects in social interaction and repetitive behavior,[21] and the potential impact of long-term therapy has been anticipated.[2]

Astroglia form a metabolic interface between the blood and the brain. Astrocytes can oxidize FAs, and PA is an essential energy source, particularly in the developing brain.[57] Compared with controls, FXS astrocytes contained more TG species 52:3, which often contain LA, combined with PA and oleic acid (18:1). The TG species 52:3 serves as a safe carrier for unsaturated FAs while limiting lipotoxicity of free SFAs, such as PA, in FXS astrocytes. On the other hand, PA-rich TG species 48:1, which include two PA residues combined with palmitoleic acid 16:1, may reflect more active *de novo* PA synthesis and SCD1 desaturation of SFAs in control astrocytes compared with FXS astrocytes. Since PA promotes insulin resistance and inflammation,[26] high plasma PA levels in *Fmr1* KO plasma are consistent with defective insulin signaling and lipolysis of storage lipid observed in models of FXS.[25,58] Additionally, there is also evidence that augmented insulin signaling may regulate neuroblast activation via glial cells in the *Drosophila* model of FXS.[59]

A shift within the n-6 PUFA pathway, favoring the conversion of AA to n-6 DPA, reduces cellular AA load. This conversion depends on Δ6-D, which incorporates the final double bond to both n-6 DPA and DHA. Since Δ6-D also initiates the pathway by inserting the first double bonds to ALA and LA precursors, many PUFAs, presenting either the precursors or products on the pathway, regulate Δ6-D activity.[60] Excess AA suppresses the synthesis of DHA by inhibiting Δ6-D and by outcompeting the n-3 family intermediates for elongases. In contrast, the excess AA improves precursor availability, thus upregulating

the synthesis of n-6 DPA. The conversion of AA to n-6 DPA serves as a mechanism to limit AA-triggered inflammation. This alleviation of AA-induced inflammation could be potentiated by n-6 DPA, which is regarded as a precursor for anti-inflammatory lipid mediators.[61] However, this emergency brake against neuroinflammation comes at a functional cost, as the structural integrity of synaptic vesicles and neurotransmission is impaired when compared with adequate brain DHA supply.[62] Currently, the effects of n-6 DPA have been studied less than the extensively investigated anti-inflammatory and neuroprotective properties of n-3 PUFAs, EPA and DHA.[63,64] The effects of n-3 PUFAs have been shown to be context dependent and modulated by brain region, animal age, and type of stimuli.[65]

The incorporation of PUFAs into membrane structures or storage lipid droplets has a role in modulating the organization of organelles within microglia, thereby influencing their capacity to regulate homeostasis, plasticity, and phagocytic abilities.[66] The n-3 DPA may shift microglial polarization toward the beneficial M2 phenotype that promotes the clearance of cellular debris, resolution of local inflammation, and the release of trophic factors that foster recovery after neurological injury.[47] Recent studies indicate a contribution of increased microglial BDNF expression in M2 microglia to the manifestation of autism.[67] We found that n-6 DPA can induce microglial *BDNF* expression in a dose-dependent manner. ACM of FXS and control astrocytes did not induce microglial *BDNF* expression, but when the astrocytes were primed with ATRA, the ACM of both FXS and control cells reduced expression of inflammatory M1 genes and showed a tendency to increase *BDNF* expression in microglia. The expression of pro-inflammatory markers did not differ in microglia cultured with FXS and control ACM, suggesting that n-6 DPA contributed to homeostatic mechanisms to control inflammatory responses in microglia. Our previous studies have shown that the levels of anti-inflammatory interleukins IL-10 and IL-13 are clearly reduced, whereas other cytokines and chemokines show minor changes in ACM of FXS astrocytes.[68] The anti-inflammatory effect of n-6 DPA on *IL1B* appeared clear even after treatment with the smallest dose. The results of n-6 DPA on *TNF* expression were inconclusive, and several inflammation-related factors may act in coordination with n-6 DPA to modulate microglial inflammatory responses and overall inflammatory states in the brain. ATRA suppresses both pro- and anti-inflammatory factors in human astrocytes,[69] and ACM from ATRA-treated astrocytes increased *BDNF* expression in the microglia, which we showed to express fewer pro-inflammatory factors. Based on the effects of exogenous n-6 DPA on microglial *BDNF* expression, the increase in n-6 DPA in FXS ACM contributed to the maintenance of the control *BDNF* expression level in nonactivated microglia. Besides modifying the release of n-6 DPA and several inflammation-related factors, ATRA regulates the secretion of trophic molecules.[28] Consequently, when either FXS or control astrocytes were treated with ATRA, their ACM triggered similar *BDNF* expression in microglia.

ATRA may, through changes in PUFA metabolism, modulate astrocyte function and secretome, affecting microglial phagocytosis and pruning of synapses that are shown to be impaired in FXS[46] as well as in autism.[52] RAs are naturally occurring metabolites of retinol (vitamin A)[70] and bind to an RAR/RXR heterodimer, which also serves as a receptor for PUFAs.[38] In addition, the three PPAR subtypes present in astrocytes and microglia bind PUFAs and form heterodimers with RXR.[71] The data suggest that the heterodimer nuclear receptors requiring both ligands are important mediators of the signaling between astrocytes and microglia.

FMRP is not essential for RA production, but FMRP interacts with RA receptor alpha (RARα),[72] and impaired RA signaling in *Fmr1* KO mice results in defective synaptic scaling, a form of homeostatic synaptic plasticity.[73] RA supplementation ameliorates mouse autism-like behaviors caused by repression in RA signaling.[74] It also rescues the atypical novelty behavior and normalizes expression of neuronal genes but fails to alleviate the defects in sociability behavior and hyperactivity in *Fmr1* KO mice,[37] possibly due to improper PUFA signaling.

We found that ATRA treatment prevented the increase in n-6 DPA in the secretome of FXS hiPSC-derived astrocytes. ATRA also modulated the expression of FA transporters and lipid metabolism in astrocytes. Like natural RA, ATRA drives the receptor complex to initiate transcriptional changes that redirect n-6 PUFAs from storage toward membrane remodeling and AA-derived signaling. In epithelial cells, ATRA has been reported to increase the *de novo* synthesis of FAs, leading to an increase in the ratio of SFAs to monounsaturated FAs and PUFAs, but also favoring n-3 PUFAs over n-6 PUFAs.[39] ATRA treatment has also been shown to induce the release of AA from astrocytes by increasing Ca^{2+}-dependent phospholipase activity.[75] We showed that the content of other FAs aside from n-6 DPA was not affected in FXS ACM. ATRA attenuated $[Ca^{2+}]_i$ signaling in FXS astrocytes, and changes in membrane PUFA composition likely influenced the balance between the structure and function of integral membrane proteins and ion channels,[42] contributing to the reduced ATP response in FXS astrocytes. The high variation of astrocytic $[Ca^{2+}]_i$ responses to ATP apparently reflected functionally different astrocyte subpopulations.[76]

Our study suggests that altered PUFA metabolism significantly contributes to the pathophysiology of FXS and that the mechanisms involved are shared with autism.[77,78] Because BDNF has a central role in neuropsychiatric and neurodegenerative pathologies, it is vital to elucidate microglial BDNF regulation, which drives neuronal plasticity. The potential of n-6 DPA to regulate microglial BDNF expression provides a unique astrocyte-dependent mechanism to modulate microglial function and new insight into the understanding of developmental processes leading to the phenotype of FXS.[79] Increased astrocytic release of n-6 DPA can fine-tune the trophic support provided by microglia. Through the action of various immune regulators, the microglial modulation ultimately sensitizes hippocampal synaptic plasticity to inflammatory stimuli.[80]

Although human astrocytes comprised functionally different subpopulations with cell line-dependent variability in the expression of many genes involved in maintaining lipid homeostasis, FXS and control astrocytes showed similar uptake of essential PUFA progenitors ALA and LA from defined culture medium. However, differences observed in the lipidomes of patient-derived FXS astrocytes indicate a need for further research involving larger cohorts of patient-specific hiPSC-derived astrocyte lines. This research could enhance understanding of the

genetic variation in homeostatic mechanisms involved in maintaining FA balance and its possible contribution to the variability in the FXS phenotype. Nevertheless, the current study's results underscore the role of PUFA signaling as part of a comprehensive treatment strategy in FXS. In addition, the involvement of PA, the levels of which may increase in circulation due to FXS-induced lipolysis[25] with consequent toxic and inflammatory effects, calls for trials where the n-3 PUFA defect and the overall metabolic dysfunction are treated at the same time. Since mutated *Fmr1* has been proposed to influence insulin and sugar metabolism, catabolism of lipids, and protein synthesis, metformin treatment is one of the candidate drugs that could be tested with n-3 PUFA supplements to correct FXS-induced metabolic and functional dysfunctions.[25,81,82]

Limitations of the study

This study has certain limitations that should be acknowledged. First, the altered molecular mechanisms have been observed in cell-based model systems, and the relevance of the findings remains to be explored *in vivo*. Second, although biological replicates allowed identification of statistically significant FXS-specific alterations, many cell line-dependent differences were found, indicating the need for further studies using more patient-derived and control cell lines. Third, the current study focused particularly on FA-related alterations, and broader analysis of FXS-dependent changes in astrocyte differentiation to functional subpopulations is limited. Furthermore, the present study fails to capture in its entirety the well-known differences between RNA and protein expression in functional subpopulations of astrocytes, which increase the complexity of the studied system beyond the scope of this study.

RESOURCE AVAILABILITY

Lead contact

Requests for further information and resources should be directed to and will be fulfilled by the lead contact, Maija L. Castrén (maija.castren@helsinki.fi).

Materials availability

This study did not generate new, unique reagents, materials, or experimental models.

Data and code availability

- The raw reads can be obtained from the European Nucleotide Archive: PRJEB110867. The count tables and other processed data are available at Zenodo: https://doi.org/10.5281/zenodo.19322443.
- The code for analyzing the scRNA-seq dataset is available at GitHub: https://github.com/DimitriMeistermann/Gerasymchuk2026.
- Any additional information required to reanalyze the data reported in this paper is available from the lead contact upon request.

ACKNOWLEDGMENTS

We thank Dr. Ulla-Kaisa Peteri for contributing to the culturing of the initial hiPSC-derived astrocyte lines and the Neural iPSC unit (NIPS) of Helsinki Institute of Life Science (HiLIFE) at the University of Helsinki for providing services and facilities for human astrocyte studies. The Single-Cell Analytics unit of the Institute for Molecular Medicine Finland (FIMM) at the University of Helsinki, supported by HiLIFE and Biocenter Finland, provided the scRNA-seq service. We used BioRender software to prepare multiple schematics included in this paper. This work was supported by FRAXA Foundation, USA, and Jane and Aatos Erkko Foundation, Finland.

AUTHOR CONTRIBUTIONS

M.L.C. conceived the study. R.K., I.M.E., M.K., M.H., H.R., J.K., and M.L.C. contributed to study design and methodology. D.G., K.T., A.H.H., M.K., and A.S.P. performed experiments and collected data. D.G., K.T., D.M., A.H.H., I.K., J.P., R.K., and M.L.C. contributed to formal analysis of data. M.L.C. and R.K. wrote the original draft, and all authors additionally contributed to the review and editing of the final paper. R.K., J.K., and M.L.C. supervised the study. M.L.C. obtained funding and provided resources for the project.

DECLARATION OF INTERESTS

The authors declare no competing interests.

DECLARATION OF GENERATIVE AI AND AI-ASSISTED TECHNOLOGIES IN THE MANUSCRIPT PREPARATION PROCESS

During the preparation of the final version of the manuscript, the authors used GPT-5 (OpenAI) and Avidnote AI in order to improve fluency and readability. After using these tools, the authors reviewed and take full responsibility for the content of the published article.

STAR★METHODS

Detailed methods are provided in the online version of this paper and include the following:

- KEY RESOURCES TABLE
- EXPERIMENTAL MODELS AND STUDY PARTICIPANT DETAILS
  - Human astrocytes
  - Human microglia
  - Mouse plasma samples
- METHOD DETAILS
  - Immunocytochemistry
  - Cell viability assay
  - Bulk RNA sequencing
  - Astrocyte conditioned medium (ACM)
  - LC-MS/MS untargeted lipidomics of astrocyte media
  - LC-MS/MS untargeted lipidomics of astrocytes
  - GC-FID and GC-MS of mouse plasma FAs
  - Single-cell RNA sequencing (scRNA-seq)
  - Analysis of scRNA-seq data
  - RNA extraction and quantitative RT-PCR analysis
  - Western blot analysis
  - Calcium imaging
- QUANTIFICATION AND STATISTICAL ANALYSIS

SUPPLEMENTAL INFORMATION

Supplemental information can be found online at https://doi.org/10.1016/j.isci.2026.118176.

Received: June 24, 2026
Revised: September 18, 2026
Accepted: October 23, 2026

REFERENCES

1. Hagerman, R.J., Berry-Kravis, E., Hazlett, H.C., Bailey, D.B., Jr., Moine, H., Kooy, R.F., Tassone, F., Gantois, I., Sonenberg, N., Mandel, J.L., and Hagerman, P.J. (2017). Fragile X syndrome. Nat. Rev. Dis. Primers *3*, 17065. https://doi.org/10.1038/nrdp.2017.65.
2. Kaufmann, W.E., Kidd, S.A., Andrews, H.F., Budimirovic, D.B., Esler, A., Haas-Givler, B., Stackhouse, T., Riley, C., Peacock, G., Sherman, S.L., et al. (2017). Autism Spectrum Disorder in Fragile X Syndrome: Cooccurring

Conditions and Current Treatment. Pediatrics *139*, S194–S206. https://doi.org/10.1542/peds.2016-1159F.

3. Verkerk, A.J., Pieretti, M., Sutcliffe, J.S., Fu, Y.-H., Kuhl, D.P., Pizzuti, A., Reiner, O., Richards, S., Victoria, M.F., Zhang, F.P., et al. (1991). Identification of a gene (FMR-1) containing a CGG repeat coincident with a breakpoint cluster region exhibiting length variation in fragile X syndrome. Cell *65*, 905–914. https://doi.org/10.1016/0092-8674(91)90397-H.
4. Santoro, M.R., Bray, S.M., and Warren, S.T. (2012). Molecular Mechanisms of Fragile X Syndrome: A Twenty-Year Perspective. Annu. Rev. Pathol. *7*, 219–245. https://doi.org/10.1146/annurev-pathol-011811-132457.
5. Darnell, J.C., Van Driesche, S.J., Zhang, C., Hung, K.Y.S., Mele, A., Fraser, C.E., Stone, E.F., Chen, C., Fak, J.J., Chi, S.W., et al. (2011). FMRP Stalls Ribosomal Translocation on mRNAs Linked to Synaptic Function and Autism. Cell *146*, 247–261. https://doi.org/10.1016/j.cell.2011.06.013.
6. Talvio, K., and Castrén, M.L. (2023). Astrocytes in fragile X syndrome. Front. Cell. Neurosci. *17*, 1322541. https://doi.org/10.3389/fncel.2023.1322541.
7. Pacey, L.K.K., and Doering, L.C. (2007). Developmental expression of FMRP in the astrocyte lineage: Implications for fragile X syndrome. Glia *55*, 1601–1609. https://doi.org/10.1002/glia.20573.
8. Lee, H.G., Wheeler, M.A., and Quintana, F.J. (2022). Function and therapeutic value of astrocytes in neurological diseases. Nat. Rev. Drug Discov. *21*, 339–358. https://doi.org/10.1038/s41573-022-00390-x.
9. Nagai, J., Yu, X., Papouin, T., Cheong, E., Freeman, M.R., Monk, K.R., Hastings, M.H., Haydon, P.G., Rowitch, D., Shaham, S., and Khakh, B.S. (2021). Behaviorally consequential astrocytic regulation of neural circuits. Neuron *109*, 576–596. https://doi.org/10.1016/j.neuron.2020.12.008.
10. Lee, J.A., Hall, B., Allsop, J., Alqarni, R., and Allen, S.P. (2021). Lipid metabolism in astrocytic structure and function. Semin. Cell Dev. Biol. *112*, 123–136. https://doi.org/10.1016/j.semcdb.2020.07.017.
11. Mallick, K., Paul, S., Banerjee, S., and Banerjee, S. (2024). Lipid Droplets and Neurodegeneration. Neuroscience *549*, 13–23. https://doi.org/10.1016/j.neuroscience.2024.04.014.
12. Moore, S.A., Yoder, E., Murphy, S., Dutton, G.R., and Spector, A.A. (1991). Astrocytes, Not Neurons, Produce Docosahexaenoic Acid (22:6ω-3) and Arachidonic Acid (20:4ω-6). J. Neurochem. *56*, 518–524. https://doi.org/10.1111/j.1471-4159.1991.tb08180.x.
13. Javanainen, M., Enkavi, G., Guixà-Gonzaléz, R., Kulig, W., Martinez-Seara, H., Levental, I., and Vattulainen, I. (2019). Reduced level of docosahexaenoic acid shifts GPCR neuroreceptors to less ordered membrane regions. PLoS Comput. Biol. *15*, e1007033. https://doi.org/10.1371/journal.pcbi.1007033.
14. Incontro, S., Musella, M.L., Sammari, M., Di Scala, C., Fantini, J., and Debanne, D. (2025). Lipids shape brain function through ion channel and receptor modulations: physiological mechanisms and clinical perspectives. Physiol. Rev. *105*, 137–207. https://doi.org/10.1152/physrev.00004.2024.
15. Liu, J., Green, P., Mann, J., and Rapoport, S. (2014). Pathways of Polyunsaturated Fatty Acid Utilization: Implications for Brain Function in Neuropsychiatric Health and Disease. Brain Res. *1597*, 220–246. https://doi.org/10.1016/j.brainres.2014.11.059.
16. Neuringer, M., Connor, W.E., Lin, D.S., Barstad, L., and Luck, S. (1986). Biochemical and Functional Effects of Prenatal and Postnatal omega 3 Fatty Acid Deficiency on Retina and Brain in Rhesus Monkeys. Proc. Natl. Acad. Sci. USA *83*, 4021–4025. https://doi.org/10.1073/pnas.83.11.4021.
17. Coti Bertrand, P., O'Kusky, J.R., and Innis, S.M. (2006). Maternal Dietary (n-3) Fatty Acid Deficiency Alters Neurogenesis in the Embryonic Rat Brain12. J. Nutr. *136*, 1570–1575. https://doi.org/10.1093/jn/136.6.1570.
18. Novak, E.M., Dyer, R.A., and Innis, S.M. (2008). High dietary ω-6 fatty acids contribute to reduced docosahexaenoic acid in the developing brain and inhibit secondary neurite growth. Brain Res. *1237*, 136–145. https://doi.org/10.1016/j.brainres.2008.07.107.
19. Innes, J.K., and Calder, P.C. (2018). Omega-6 fatty acids and inflammation. Prostaglandins Leukot. Essent. Fatty Acids *132*, 41–48. https://doi.org/10.1016/j.plefa.2018.03.004.
20. Abolghasemi, A., Carullo, M.P., Aguilera, E.C., Laroui, A., Plantefeve, R., Rojas, D., Benachenhou, S., Ramírez, M.V., Proteau-Lemieux, M., Lepage, J.F., et al. (2022). Alteration of Fatty Acid Profile in Fragile X Syndrome. Int. J. Mol. Sci. *23*, 10815. https://doi.org/10.3390/ijms231810815.
21. Mazahery, H., Stonehouse, W., Delshad, M., Kruger, M.C., Conlon, C.A., Beck, K.L., and Von Hurst, P.R. (2017). Relationship between Long Chain n-3 Polyunsaturated Fatty Acids and Autism Spectrum Disorder: Systematic Review and Meta-Analysis of Case-Control and Randomised Controlled Trials. Nutrients *9*, 155. https://doi.org/10.3390/nu9020155.
22. Pietropaolo, S., Goubran, M.G., Joffre, C., Aubert, A., Lemaire-Mayo, V., Crusio, W.E., and Layé, S. (2014). Dietary supplementation of omega-3 fatty acids rescues fragile X phenotypes in Fmr1-Ko mice. Psychoneuroendocrinology *49*, 119–129. https://doi.org/10.1016/j.psyneuen.2014.07.002.
23. Schiavi, S., Carbone, E., Melancia, F., Buzzelli, V., Manduca, A., Campolongo, P., Pallottini, V., and Trezza, V. (2022). Perinatal supplementation with omega-3 fatty acids corrects the aberrant social and cognitive traits observed in a genetic model of autism based on FMR1 deletion in rats. Nutr. Neurosci. *25*, 898–911. https://doi.org/10.1080/1028415X.2020.1819107.
24. Nolan, S.O., Hodges, S.L., Binder, M.S., Smith, G.D., Okoh, J.T., Jefferson, T.S., Escobar, B., and Lugo, J.N. (2022). Dietary rescue of adult behavioral deficits in the Fmr1 knockout mouse. PLoS One *17*, e0262916. https://doi.org/10.1371/journal.pone.0262916.
25. Leboucher, A., Pisani, D.F., Martinez-Gili, L., Chilloux, J., Bermudez-Martin, P., Van Dijck, A., Ganief, T., Macek, B., Becker, J.A.J., Le Merrer, J., et al. (2019). The translational regulator FMRP controls lipid and glucose metabolism in mice and humans. Mol. Metab. *21*, 22–35. https://doi.org/10.1016/j.molmet.2019.01.002.
26. Amine, H., Benomar, Y., and Taouis, M. (2021). Palmitic acid promotes resistin-induced insulin resistance and inflammation in SH-SY5Y human neuroblastoma. Sci. Rep. *11*, 5427. https://doi.org/10.1038/s41598-021-85018-7.
27. Qadir, A.M., Omar, R.A., Sulaiman, S.H., and Barzani, H.A.H. (2026). Brain lipid metabolism and transport: implications for neurodegeneration and therapeutic strategies: a comprehensive review. Metab. Brain Dis. *41*, 14. https://doi.org/10.1007/s11011-025-01778-5.
28. Peteri, U.-K., Pitkonen, J., de Toma, I., Nieminen, O., Utami, K.H., Strandin, T.M., Corcoran, P., Roybon, L., Vaheri, A., Ethell, I., et al. (2021). Urokinase plasminogen activator mediates changes in human astrocytes modeling fragile X syndrome. Glia *69*, 2947–2962. https://doi.org/10.1002/glia.24080.
29. Escartin, C., Pierre, K., Colin, A., Brouillet, E., Delzescaux, T., Guillermier, M., Dhenain, M., Déglon, N., Hantraye, P., Pellerin, L., and Bonvento, G. (2007). Activation of Astrocytes by CNTF Induces Metabolic Plasticity and Increases Resistance to Metabolic Insults. J. Neurosci. *27*, 7094–7104. https://doi.org/10.1523/JNEUROSCI.0174-07.2007.
30. Peteri, U.-K., Pitkonen, J., Utami, K.H., Paavola, J., Roybon, L., Pouladi, M.A., and Castrén, M.L. (2021). Generation of the Human Pluripotent Stem-Cell-Derived Astrocyte Model with Forebrain Identity. Brain Sci. *11*, 209. https://doi.org/10.3390/brainsci11020209.
31. Liddelow, S.A., and Barres, B.A. (2017). Reactive Astrocytes: Production, Function, and Therapeutic Potential. Immunity *46*, 957–967. https://doi.org/10.1016/j.immuni.2017.06.006.
32. Talvio, K., Minkeviciene, R., Townsley, K.G., Achuta, V.S., Huckins, L.M., Corcoran, P., Brennand, K.J., and Castrén, M.L. (2022). Reduced LYNX1 expression in transcriptome of human iPSC-derived neural progenitors modeling fragile X syndrome. Front. Cell Dev. Biol. *10*, 1034679. https://doi.org/10.3389/fcell.2022.1034679.
33. Lee-Okada, H.C., Xue, C., and Yokomizo, T. (2025). Recent advances on the physiological and pathophysiological roles of polyunsaturated fatty

acids and their biosynthetic pathway. Biochim. Biophys. Acta. Mol. Cell Biol. Lipids *1870*, 159564. https://doi.org/10.1016/j.bbalip.2024.159564.

34. Telias, M., Mayshar, Y., Amit, A., and Ben-Yosef, D. (2015). Molecular mechanisms regulating impaired neurogenesis of fragile X syndrome human embryonic stem cells. Stem Cells Dev. *24*, 2353–2365. https://doi.org/10.1089/scd.2015.0220.

35. Brighi, C., Salaris, F., Soloperto, A., Cordella, F., Ghirga, S., de Turris, V., Rosito, M., Porceddu, P.F., D'Antoni, C., Reggiani, A., et al. (2021). Novel fragile X syndrome 2D and 3D brain models based on human isogenic FMRP-KO iPSCs. Cell Death Dis. *12*, 498. https://doi.org/10.1038/s41419-021-03776-8.

36. Hatch, G.M., Smith, A.J., Xu, F.Y., Hall, A.M., and Bernlohr, D.A. (2002). FATP1 channels exogenous FA into 1,2,3-triacyl-sn-glycerol and down-regulates sphingomyelin and cholesterol metabolism in growing 293 cells. J. Lipid Res. *43*, 1380–1389. https://doi.org/10.1194/jlr.M200130-JLR200.

37. Yang, L., Xia, Z., Feng, J., Zhang, M., Miao, P., Nie, Y., Zhang, X., Hao, Z., and Hu, R. (2022). Retinoic Acid Supplementation Rescues the Social Deficits in Fmr1 Knockout Mice. Front. Genet. *13*, 928393. https://doi.org/10.3389/fgene.2022.928393.

38. Lengqvist, J., Mata De Urquiza, A., Bergman, A.C., Willson, T.M., Sjövall, J., Perlmann, T., and Griffiths, W.J. (2004). Polyunsaturated fatty acids including docosahexaenoic and arachidonic acid bind to the retinoid X receptor alpha ligand-binding domain. Mol. Cell. Proteomics *3*, 692–703. https://doi.org/10.1074/mcp.M400003-MCP200.

39. Liao, X.D., Zhou, C.H., Zhang, J., Shen, J.L., Wang, Y.J., Jin, Y.C., and Li, S.L. (2020). Effect of all-trans retinoic acid on casein and fatty acid synthesis in MAC-T cells. Asian-Australas. J. Anim. Sci. *33*, 1012–1022. https://doi.org/10.5713/ajas.19.0315.

40. Kubickova, B., Martinkova, S., Bohaciakova, D., Nezvedova, M., Liu, R., Brozman, O., Spáčil, Z., and Hilscherova, K. (2023). Effects of all-trans and 9-cis retinoic acid on differentiating human neural stem cells in vitro. Toxicology *487*, 153461. https://doi.org/10.1016/j.tox.2023.153461.

41. Zhang, W., Levi, L., Banerjee, P., Jain, M., and Noy, N. (2015). Kruppel-like factor 2 suppresses mammary carcinoma growth by regulating retinoic acid signaling. Oncotarget *6*, 35830–35842. https://doi.org/10.18632/oncotarget.5767.

42. Eldho, N.V., Feller, S.E., Tristram-Nagle, S., Polozov, I.V., and Gawrisch, K. (2003). Polyunsaturated Docosahexaenoic vs Docosapentaenoic AcidDifferences in Lipid Matrix Properties from the Loss of One Double Bond. J. Am. Chem. Soc. *125*, 6409–6421. https://doi.org/10.1021/ja029029o.

43. Teshima, R., Amano, F., Nakamura, R., Tanaka, Y., and Sawada, J.-i. (2007). Effects of polyunsaturated fatty acids on calcium response and degranulation from RBL-2H3 cells. Int. Immunopharmacol. *7*, 205–210. https://doi.org/10.1016/j.intimp.2006.09.017.

44. Bazargani, N., and Attwell, D. (2016). Astrocyte calcium signaling: The third wave. Nat. Neurosci. *19*, 182–189. https://doi.org/10.1038/nn.4201.

45. Parrott, J.M., Oster, T., and Lee, H.Y. (2021). Altered inflammatory response in FMRP-deficient microglia. iScience *24*, 103293. https://doi.org/10.1016/j.isci.2021.103293.

46. Jawaid, S., Kidd, G.J., Wang, J., Swetlik, C., Dutta, R., and Trapp, B.D. (2018). Alterations in CA1 hippocampal synapses in a mouse model of fragile X syndrome. Glia *66*, 789–800. https://doi.org/10.1002/glia.23284.

47. Liu, B., Zhang, Y., Yang, Z., Liu, M., Zhang, C., Zhao, Y., and Song, C. (2021). ω-3 DPA Protected Neurons from Neuroinflammation by Balancing Microglia M1/M2 Polarizations through Inhibiting NF-κB/MAPK p38 Signaling and Activating Neuron-BDNF-PI3K/AKT Pathways. Mar. Drugs *19*, 587. https://doi.org/10.3390/md19110587.

48. Schmitz, G., and Ecker, J. (2008). The opposing effects of n−3 and n−6 fatty acids. Prog. Lipid Res. *47*, 147–155. https://doi.org/10.1016/j.plipres.2007.12.004.

49. Cleland, N.R.W., and Bruce, K.D. (2024). Fatty acid sensing in the brain: The role of glial-neuronal metabolic crosstalk and horizontal lipid flux. Biochimie *223*, 166–178. https://doi.org/10.1016/j.biochi.2022.08.012.

50. De Carvalho, C.C.C.R., and Caramujo, M.J. (2018). The Various Roles of Fatty Acids. Molecules *23*, 2583. https://doi.org/10.3390/molecules23102583.

51. Traetta, M.E., Vecchiarelli, H.A., and Tremblay, M.È. (2025). Fundamental Neurochemistry Review: Lipids across microglial states. J. Neurochem. *169*, e16259. https://doi.org/10.1111/jnc.16259.

52. Kim, H.J., Cho, M.H., Shim, W.H., Kim, J.K., Jeon, E.Y., Kim, D.H., and Yoon, S.Y. (2017). Deficient autophagy in microglia impairs synaptic pruning and causes social behavioral defects. Mol. Psychiatry *22*, 1576–1584. https://doi.org/10.1038/mp.2016.103.

53. Barber, C.N., and Raben, D.M. (2019). Lipid Metabolism Crosstalk in the Brain: Glia and Neurons. Front. Cell. Neurosci. *13*, 212. https://doi.org/10.3389/fncel.2019.00212.

54. Bazinet, R.P., and Layé, S. (2014). Polyunsaturated fatty acids and their metabolites in brain function and disease. Nat. Rev. Neurosci. *15*, 771–785. https://doi.org/10.1038/nrn3820.

55. Ferrero, E., Vaz, F.M., Cheillan, D., Brusco, A., and Marelli, C. (2025). The ELOVL proteins: Very and ultra long-chain fatty acids at the crossroads between metabolic and neurodegenerative disorders. Mol. Genet. Metab. *144*, 109050. https://doi.org/10.1016/j.ymgme.2025.109050.

56. Parletta, N., Niyonsenga, T., and Duff, J. (2016). Omega-3 and Omega-6 Polyunsaturated Fatty Acid Levels and Correlations with Symptoms in Children with Attention Deficit Hyperactivity Disorder, Autistic Spectrum Disorder and Typically Developing Controls. PLoS One *11*, e0156432. https://doi.org/10.1371/journal.pone.0156432.

57. Edmond, J., Robbins, R.A., Bergstrom, J.D., Cole, R.A., and de Vellis, J. (1987). Capacity for substrate utilization in oxidative metabolism by neurons, astrocytes, and oligodendrocytes from developing brain in primary culture. J. Neurosci. Res. *18*, 551–561. https://doi.org/10.1002/jnr.490180407.

58. Weisz, E.D., Towheed, A., Monyak, R.E., Toth, M.S., Wallace, D.C., and Jongens, T.A. (2018). Loss of Drosophila FMRP leads to alterations in energy metabolism and mitochondrial function. Hum. Mol. Genet. *27*, 95–106. https://doi.org/10.1093/hmg/ddx387.

59. Callan, M.A., Clements, N., Ahrendt, N., and Zarnescu, D.C. (2012). Fragile X Protein is required for inhibition of insulin signaling and regulates glial-dependent neuroblast reactivation in the developing brain. Brain Res. *1462*, 151–161. https://doi.org/10.1016/j.brainres.2012.03.042.

60. Valenzuela, R., Metherel, A.H., Cisbani, G., Smith, M.E., Chouinard-Watkins, R., Klievik, B.J., Farias, C., Videla, L.A., and Bazinet, R.P. (2025). Specific activity of mouse liver desaturases and elongases: Time course effects using n-3 and n-6 PUFA substrates and inhibitory responses of delta-6 desaturase. Biochim. Biophys. Acta. Mol. Cell Biol. Lipids *1870*, 159594. https://doi.org/10.1016/j.bbalip.2025.159594.

61. Ma, Q.L., Zhu, C., Morselli, M., Su, T., Pelligrini, M., Lu, Z., Jones, M., Denver, P., Castro, D., Gu, X., et al. (2020). The Novel Omega-6 Fatty Acid Docosapentaenoic Acid Positively Modulates Brain Innate Immune Response for Resolving Neuroinflammation at Early and Late Stages of Humanized APOE-Based Alzheimer's Disease Models. Front. Immunol. *11*, 558036. https://doi.org/10.3389/fimmu.2020.558036.

62. Sidhu, V.K., Huang, B.X., Desai, A., Kevala, K., and Kim, H.-Y. (2016). Role of DHA in aging-related changes in mouse brain synaptic plasma membrane proteome. Neurobiol. Aging *41*, 73–85. https://doi.org/10.1016/j.neurobiolaging.2016.02.007.

63. Serhan, C.N., Gotlinger, K., Hong, S., and Arita, M. (2004). Resolvins, docosatrienes, and neuroprotectins, novel omega-3-derived mediators, and their aspirin-triggered endogenous epimers: an overview of their

protective roles in catabasis. Prostaglandins Other Lipid Mediat. *73*, 155–172. https://doi.org/10.1016/j.prostaglandins.2004.03.005.

64. Xia, J., Yang, L., Huang, C., Deng, S., Yang, Z., Zhang, Y., Zhang, C., and Song, C. (2023). Omega-3 Polyunsaturated Fatty Acid Eicosapentaenoic Acid or Docosahexaenoic Acid Improved Ageing-Associated Cognitive Decline by Regulating Glial Polarization. Mar. Drugs *21*, 398. https://doi.org/10.3390/md21070398.
65. Drouin, G., Rioux, V., and Legrand, P. (2019). The n-3 docosapentaenoic acid (DPA): A new player in the n-3 long chain polyunsaturated fatty acid family. Biochimie *159*, 36–48. https://doi.org/10.1016/j.biochi.2019.01.022.
66. Tremblay, M.-E., Zhang, I., Bisht, K., Savage, J.C., Lecours, C., Parent, M., Titorenko, V., and Maysinger, D. (2016). Remodeling of lipid bodies by docosahexaenoic acid in activated microglial cells. J. Neuroinflammation *13*, 116. https://doi.org/10.1186/s12974-016-0580-0.
67. Komori, T., Okamura, K., Ikehara, M., Yamamuro, K., Endo, N., Okumura, K., Yamauchi, T., Ikawa, D., Ouji-Sageshima, N., Toritsuka, M., et al. (2024). Brain-derived neurotrophic factor from microglia regulates neuronal development in the medial prefrontal cortex and its associated social behavior. Mol. Psychiatry *29*, 1338–1349. https://doi.org/10.1038/s41380-024-02413-y.
68. Talvio, K., Wagner, V.A., Minkeviciene, R., Kirkwood, J.S., Kulinich, A.O., Umemori, J., Bhatia, A., Hur, M., Käkelä, R., Ethell, I.M., and Castrén, M.L. (2023). An iPSC-derived astrocyte model of fragile X syndrome exhibits dysregulated cholesterol homeostasis. Commun. Biol. *6*, 789. https://doi.org/10.1038/s42003-023-05147-9.
69. Yoo, S.H., Kim, D., Yeon, G.-B., Choi, J., Lee, J., Kim, D.-W., Kim, H., and Kim, D.-S. (2026). Retinoic acid signaling regulates astrocyte reactivity by modulating MAPK/NF-κB pathways and mitochondrial integrity. Neurochem. Int. *194*, 106134. https://doi.org/10.1016/j.neuint.2026.106134.
70. Kumar, S., and Duester, G. (2011). SnapShot: Retinoic Acid Signaling. Cell *147*, 1422–1422.e1. https://doi.org/10.1016/j.cell.2011.11.034.
71. Kilu, W., Merk, D., Steinhilber, D., Proschak, E., and Heering, J. (2021). Heterodimer formation with retinoic acid receptor RXRalpha modulates coactivator recruitment by peroxisome proliferator-activated receptor PPARgamma. J. Biol. Chem. *297*, 100814. https://doi.org/10.1016/j.jbc.2021.100814.
72. Park, E., Lau, A.G., Arendt, K.L., and Chen, L. (2021). FMRP Interacts with RARα in Synaptic Retinoic Acid Signaling and Homeostatic Synaptic Plasticity. Int. J. Mol. Sci. *22*, 6579. https://doi.org/10.3390/ijms22126579.
73. Zhang, Z., Marro, S.G., Zhang, Y., Arendt, K.L., Patzke, C., Zhou, B., Fair, T., Yang, N., Südhof, T.C., Wernig, M., and Chen, L. (2018). The fragile X mutation impairs homeostatic plasticity in human neurons by blocking synaptic retinoic acid signaling. Sci. Transl. Med. *10*, eaar4338. https://doi.org/10.1126/scitranslmed.aar4338.
74. Xu, X., Li, C., Gao, X., Xia, K., Guo, H., Li, Y., Hao, Z., Zhang, L., Gao, D., Xu, C., et al. (2018). Excessive UBE3A dosage impairs retinoic acid signaling and synaptic plasticity in autism spectrum disorders. Cell Res. *28*, 48–68. https://doi.org/10.1038/cr.2017.132.
75. Farooqui, A.A., Antony, P., Ong, W.-Y., Horrocks, L.A., and Freysz, L. (2004). Retinoic acid-mediated phospholipase A2 signaling in the nucleus. Brain Res. Rev. *45*, 179–195. https://doi.org/10.1016/j.brainresrev.2004.03.002.
76. Reddy, B.K., Annaiyappa, N., Bhattacharya, A., Chattarji, S., and Pal, R. (2025). Generation and Characterization of Human Induced Pluripotent Stem Cell-derived Astrocytes Lacking Fragile X Messenger Ribonucleoprotein. JoVE J. e68081. https://doi.org/10.3791/68081.
77. Martínez-Cerdeño, V. (2017). Dendrite and spine modifications in autism and related neurodevelopmental disorders in patients and animal models. Dev. Neurobiol. *77*, 393–404. https://doi.org/10.1002/dneu.22417.
78. Cruz-Martín, A., Crespo, M., and Portera-Cailliau, C. (2010). Delayed Stabilization of Dendritic Spines in Fragile X Mice. J. Neurosci. *30*, 7793–7803. https://doi.org/10.1523/JNEUROSCI.0577-10.2010.
79. Morin-Parent, F., Champigny, C., Lacroix, A., Corbin, F., and Lepage, J.-F. (2019). Hyperexcitability and impaired intracortical inhibition in patients with fragile-X syndrome. Transl. Psychiatry *9*, 312. https://doi.org/10.1038/s41398-019-0650-z.
80. Delpech, J.C., Thomazeau, A., Madore, C., Bosch-Bouju, C., Larrieu, T., Lacabanne, C., Remus-Borel, J., Aubert, A., Joffre, C., Nadjar, A., and Layé, S. (2015). Dietary n-3 PUFAs Deficiency Increases Vulnerability to Inflammation-Induced Spatial Memory Impairment. Neuropsychopharmacology *40*, 2774–2787. https://doi.org/10.1038/npp.2015.127.
81. Dy, A.B.C., Tassone, F., Eldeeb, M., Salcedo-Arellano, M.J., Tartaglia, N., and Hagerman, R. (2018). Metformin as targeted treatment in fragile X syndrome. Clin. Genet. *93*, 216–222. https://doi.org/10.1111/cge.13039.
82. Utami, K.H., Yusof, N.A.B.M., Kwa, J.E., Peteri, U.K., Castrén, M.L., and Pouladi, M.A. (2020). Elevated de novo protein synthesis in FMRP-deficient human neurons and its correction by metformin treatment. Mol. Autism *11*, 41. https://doi.org/10.1186/s13229-020-00350-5.
83. Amezquita, R.A., Lun, A.T.L., Becht, E., Carey, V.J., Carpp, L.N., Geistlinger, L., Marini, F., Rue-Albrecht, K., Risso, D., Soneson, C., et al. (2020). Orchestrating single-cell analysis with Bioconductor. Nat. Methods *17*, 137–145. https://doi.org/10.1038/s41592-019-0654-x.
84. Love, M.I., Huber, W., and Anders, S. (2014). Moderated estimation of fold change and dispersion for RNA-seq data with DESeq2. Genome Biol. *15*, 550. https://doi.org/10.1186/s13059-014-0550-8.
85. Hu, B., Jin, J., Guo, A.-Y., Zhang, H., Luo, J., and Gao, G. (2015). GSDS 2.0: an upgraded gene feature visualization server. Bioinformatics *31*, 1296–1297. https://doi.org/10.1093/bioinformatics/btu817.
86. Korsunsky, I., Millard, N., Fan, J., Slowikowski, K., Zhang, F., Wei, K., Baglaenko, Y., Brenner, M., Loh, P.-r., and Raychaudhuri, S. (2019). Fast, sensitive and accurate integration of single-cell data with Harmony. Nat. Methods *16*, 1289–1296. https://doi.org/10.1038/s41592-019-0619-0.
87. Ovek Baydar, D., Rauluseviciute, I., Aronsen, D.R., Blanc-Mathieu, R., Bonthuis, I., de Beukelaer, H., Ferenc, K., Jegou, A., Kumar, V., Lemma, R.B., et al. (2026). JASPAR 2026: expansion of transcription factor binding profiles and integration of deep learning models. Nucleic Acids Res. *54*, D184–D193. https://doi.org/10.1093/nar/gkaf1209.
88. Haimi, P., Uphoff, A., Hermansson, M., and Somerharju, P. (2006). Software Tools for Analysis of Mass Spectrometric Lipidome Data. Anal. Chem. *78*, 8324–8331. https://doi.org/10.1021/ac061390w.
89. Meistermann, D. (2022). oob (GitHub). https://github.com/DimitriMeistermann/oob.
90. Dobin, A., Davis, C.A., Schlesinger, F., Drenkow, J., Zaleski, C., Jha, S., Batut, P., Chaisson, M., and Gingeras, T.R. (2013). STAR: ultrafast universal RNA-seq aligner. Bioinformatics *29*, 15–21. https://doi.org/10.1093/bioinformatics/bts635.
91. Amid, E., and Warmuth, M.K. (2019). TriMap: Large-scale dimensionality reduction using triplets. Preprint at arXiv. http://arxiv.org/abs/1910.00204.
92. McQuade, A., Coburn, M., Tu, C.H., Hasselmann, J., Davtyan, H., and Blurton-Jones, M. (2018). Development and validation of a simplified method to generate human microglia from pluripotent stem cells. Mol. Neurodegener. *13*, 67. https://doi.org/10.1186/s13024-018-0297-x.
93. Koskuvi, M., Pörsti, E., Hewitt, T., Räsänen, N., Wu, Y.-C., Trontti, K., McQuade, A., Kalyanaraman, S., Ojansuu, I., Vaurio, O., et al. (2024). Genetic contribution to microglial activation in schizophrenia. Mol. Psychiatry *29*, 2622–2633. https://doi.org/10.1038/s41380-024-02529-1.
94. Tervonen, T.A., Ajamian, F., De Wit, J., Verhaagen, J., Castrén, E., and Castrén, M. (2006). Overexpression of a truncated TrkB isoform increases the proliferation of neural progenitors. Eur. J. Neurosci. *24*, 1277–1285. https://doi.org/10.1111/j.1460-9568.2006.05010.x.
95. Hollin, T., Abel, S., Falla, A., Pasaje, C.F.A., Bhatia, A., Hur, M., Kirkwood, J.S., Saraf, A., Prudhomme, J., De Souza, A., et al. (2022). Functional

genomics of RAP proteins and their role in mitoribosome regulation in Plasmodium falciparum. Nat. Commun. *13*, 1275. https://doi.org/10.1038/s41467-022-28981-7.

96. Reddam, A., Mitchell, C.A., Dasgupta, S., Kirkwood, J.S., Vollaro, A., Hur, M., and Volz, D.C. (2019). mRNA-Sequencing Identifies Liver as a Potential Target Organ for Triphenyl Phosphate in Embryonic Zebrafish. Toxicol. Sci. *172*, 51–62. https://doi.org/10.1093/toxsci/kfz169.
97. Kind, T., Liu, K.-H., Lee, D.Y., DeFelice, B., Meissen, J.K., and Fiehn, O. (2013). LipidBlast in silico tandem mass spectrometry database for lipid identification. Nat. Methods *10*, 755–758. https://doi.org/10.1038/nmeth.2551.
98. Smith, C.A., Maille, G.O., Want, E.J., Qin, C., Trauger, S.A., Brandon, T.R., Custodio, D.E., Abagyan, R., and Siuzdak, G. (2005). METLIN: A Metabolite Mass Spectral Database. Ther. Drug Monit. *27*, 747–751. https://doi.org/10.1097/01.ftd.0000179845.53213.39.
99. Folch, J., Lees, M., and Stanley, G.H.S. (1957). A simple method for the isolation and purification of total lipides from animal tissues. J. Biol. Chem. *226*, 497–509. https://doi.org/10.1016/s0021-9258(18)64849-5.
100. Breitkopf, S.B., Ricoult, S.J.H., Yuan, M., Xu, Y., Peake, D.A., Manning, B.D., and Asara, J.M. (2017). A relative quantitative positive/negative ion switching method for untargeted lipidomics via high resolution LC-MS/MS from any biological source. Metabolomics *13*, 30. https://doi.org/10.1007/s11306-016-1157-8.
101. Fellenberg, A.J., Johnson, D.W., Poulos, A., and Sharp, P. (1987). Simple mass spectrometric differentiation of the n-3, n-6 and n-9 series of methylene interrupted polyenoic acids. Biomed. Environ. Mass Spectrom *14*, 127–129. https://doi.org/10.1002/bms.1200140306.
102. Conroy, M.J., Andrews, R.M., Andrews, S., Cockayne, L., Dennis, E.A., Fahy, E., Gaud, C., Griffiths, W.J., Jukes, G., Kolchin, M., et al. (2024). LIPID MAPS: update to databases and tools for the lipidomics community. Nucleic Acids Res. *52*, D1677–D1682. https://doi.org/10.1093/nar/gkad896.
103. Ackman, R.G. (1992). The absorption of fish oils and concentrates. Lipids *27*, 858–862. https://doi.org/10.1007/BF02535864.
104. Käkelä, R., Tanhuanpää, K., Laitinen, S., Somerharju, P., and Olkkonen, V.M. (2005). Overexpression of OSBP-related protein 2 (ORP2) in CHO cells induces alterations of phospholipid species composition. Biochem. Cell Biol *83*, 677–683. https://doi.org/10.1139/o05-056.
105. University of Helsinki (2024). SCA General Cell Preparation Protocol. https://www.helsinki.fi/en/infrastructures/single-cell-omics/sca-general-cell-preparation-protocol.
106. Wickham, H. (2009). ggplot2: Elegant Graphics for Data Analysis (Springer). https://doi.org/10.1007/978-0-387-98141-3.
107. Gu, Z., Eils, R., and Schlesner, M. (2016). Complex heatmaps reveal patterns and correlations in multidimensional genomic data. Bioinformatics *32*, 2847–2849. https://doi.org/10.1093/bioinformatics/btw313.
108. Traag, V.A., Waltman, L., and van Eck, N.J. (2019). From Louvain to Leiden: guaranteeing well-connected communities. Sci. Rep. *9*, 5233. https://doi.org/10.1038/s41598-019-41695-z.
109. Meistermann, D. (2023). GSDS (GitHub). https://github.com/DimitriMeistermann/GSDS.
110. The Gene Ontology Consortium (2026). The Gene Ontology knowledgebase in 2026. Nucleic Acids Res. *54*, D1779–D1792. https://doi.org/10.1093/nar/gkaf1292.
111. Kanehisa, M., and Goto, S. (2000). KEGG: Kyoto Encyclopedia of Genes and Genomes. Nucleic Acids Res. *28*, 27–30. https://doi.org/10.1093/nar/28.1.27.
112. Wickham, H. (2011). ggplot2. WIREs Comput. Stat. *3*, 180–185. https://doi.org/10.1002/wics.147.
113. Wickham, H., Averick, M., Bryan, J., Chang, W., McGowan, L., François, R., Grolemund, G., Hayes, A., Henry, L., Hester, J., et al. (2019). Welcome to the Tidyverse. J. Open Source Softw. *4*, 1686. https://doi.org/10.21105/joss.01686.
114. Kassambara, A., and Mundt, F. (2020). factoextra: Extract and visualize the results of multivariate data analyses (R package version 1.0.7).

STAR★METHODS

KEY RESOURCES TABLE

REAGENT or RESOURCE	SOURCE	IDENTIFIER
Antibodies		
Chicken polyclonal anti-GFAP	Abcam	Cat# 4674; RRID: AB_304558
Goat anti-rabbit IgG (H + L) HRP-conjucated antibody,	Thermo Fisher Scientific	Cat# A16096; RRID: AB_2534770
Mouse monoclonal anti-GAPDH	Millipore	Cat# MAB374; RRID: AB_2107445
Mouse monoclonal anti-S100B	Sigma-Aldrich	Cat# S2532; RRID: AB_477499
Rabbit polyclonal anti-NF1A	Active Motif	Cat# 39397; RRID: AB_2314931
Rabbit monoclonal anti-FATP1/SLC27A1	Cell Signaling Technology	Cat# 78571; RRID: AB_3752049
Rabbit anti-mouse IgG HRP-conjucated antibody	Sigma-Aldrich	Cat# A9044; RRID: AB_258431
Chemicals, peptides, and recombinant proteins		
12 Well-Plate	Thermo Fisher Scientific	Cat# 145040
24 Well-Plate	Thermo Fisher Scientific	Cat# 142475
3-(4,5-dimethyl-2-thiazolyl)-2,5-diphenyl-2H-tetrazolium bromide (MTT)	Sigma-Aldrich	Cat# M5655
37-component quantitative FAME standard	Supelco	Cat# CRM47885
4′6-diamino-2-phenylindole (DAPI)	Sigma-Aldrich	Cat# D9542
6 Well-Plate	Greiner	Cat# 657160
6 Well-Plate Low-Attachment	Corning	Cat# 3471
Advanced Dulbecco's Modified Eagle Medium (DMEM/F12)	Thermo Fisher Scientific	Cat# 12634028
All-trans retinoic acid (ATRA)	Sigma-Aldrich	Cat# R2625
B27-RA	Thermo Fisher Scientific	Cat# 12587010
Basic fibroblast growth factor (bFGF)	Peprotech	Cat# 100–188
Brain-derived neurotrophic factor (BDNF)	Peprotech	Cat# 450–02
BSA-Fatty Acid Complexes	Cayman Chemical	Cat# 34932
C17 Ceramide (d18:1/17:0)	Avanti Polar Lipids	Cat# 860517P
CD200	Biolegend	Cat# 770002
Ciliary neurotrophic factor (CNTF)	Peprotech	Cat# 450-13
Cyclopamine	Sigma-Aldrich	Cat# C4116
DKK1 (Dickkopf-related protein 1)	Peprotech	Cat# 120-30
EDTA-coated test tubes	Kabe Labortechnic Gmbh	Cat# 030204
Epidermal growth factor (EGF)	Peprotech	Cat# AF100-15
Essential 8 medium	Thermo Fisher Scientific	Cat# A1517001
Ethylenediaminetetraacetic acid (EDTA)	Invitrogen	Cat# AM9260G
Fractalkine (CX3CL1)	Peprotech	Cat# 300-31
Fura-2	HelloBio	Cat# HB0780
Glutamax	Thermo Fisher Scientific	Cat# 35050061
Heparin	Thermo Fisher Scientific	Cat# H4784
Insulin	Sigma-Aldrich	Cat# I0516
Insulin-Transferrin-Selenium (ITS-G)	Thermo Fisher Scientific	Cat# 41400045
Interleukin-34 (IL34)	Peprotech	Cat# 200-34
Laminin	Sigma-Aldrich	Cat# 114956-81-9
LDN-193189	Stemgent	Cat# 1062368
Macrophage colony stimulating factor 1 (M-CSF)	Peprotech	Cat# 315-02

(*Continued on next page*)

Continued

REAGENT or RESOURCE	SOURCE	IDENTIFIER
Matrigel	Corning	Cat# 356231
Monothioglycerol	Sigma-Aldrich	Cat# M6145
n-6 DPA complexed with bovine serum albumin (BSA)	Cayman Chemical	Cat# 44502
N2 supplement	Thermo Fisher Scientific	Cat# 17502048
Non-essential amino acid supplement (NEAA)	Thermo Fisher Scientific	Cat# 11140050
Penicillin/streptomycin	Thermo Fisher Scientific	Cat# 15070063
Pierce™ Phosphatase inhibitors	Thermo Fisher Scientific	Cat# A32957
Pierce™ Protease	Thermo Fisher Scientific	Cat# A32955
Pierce™ RIPA buffer	Thermo Fisher Scientific	Cat# 89900
Poly-ornithine	Sigma-Aldrich	Cat# 82682-33-5
PowerUp SYBR Green Master Mix	Thermo Fisher Scientific	Cat# A25780
ReLeSR	StemCell Technologies	Cat# 100-0483
RevertAid H Minus Reverse Transcriptase	Thermo Fisher Scientific	Cat# EP0451
Rho kinase inhibitor Y-27632 dihydrochloride	Sigma-Aldrich	Cat# Y0503
SB-431542	Sigma-Aldrich	Cat# S4317
SPLASH™ LIPIDOMIX™ Mass Spec Standard	Avanti Polar Lipids	Cat# A83707
T-25 (25 cm^2) Flask	Thermo Fisher Scientific	Cat# 156367
Transforming Growth Factor β 1 (TGF-betaβ-1)	Peprotech	Cat# 100-21
Trypsin-EDTA	Thermo Fisher Scientific	Cat# 25300062
ViewPlate-96	PerkinElmer	Cat# N9302560
Critical commercial assays		
Chromium Next GEM Single Cell 3' Kit v3.1	10X Genomics	Cat# PN-1000269
Pierce BCA Protein assay kit	Thermo Fisher Scientific	Cat# 23255
Pierce™ ECL Plus kit	Thermo Fisher Scientific	Cat# 32132
RNeasy Mini Kit	Qiagen	Cat# 74106
StemDiff Hematopoietic kit	StemCell Technologies	Cat# 05310
Deposited data		
Bulk RNA sequencing data	Peteri et al.[28,30]	GEO: GSE228378
Code for scRNA-seq dataset analysis	This paper	GitHub: https://github.com/DimitriMeistermann/Gerasymchuk2026
Raw scRNA-seq reads	European Nucleotide Archive	European Nucletide Archive: PRJEB110867
scRNA-seq count tables and other processed data	This paper	Zenodo: https://doi.org/10.5281/zenodo.19322443
Experimental models: cell lines		
Human iPSC-derived PO2/UEF-3A cell line from healthy donor (male)	Jari Koistinaho laboratory	Not commercially available
Human iPSC-derived PO4/UEF-3B cell line from healthy donor (male)	Jari Koistinaho laboratory	Not commercially available
Human iPSC-derived HEL23.3 cell line from healthy donor (male)	University of Helsinki	RRID: CVCL_VT42
Human iPSC-derived HEL24.3 cell line from healthy donor (male)	University of Helsinki	RRID: CVCL_9T96
Human iPSC-derived HEL46.11 cell line from healthy donor (male)	University of Helsinki	RRID: CVCL_UL37
Human iPSC-derived HEL69.5 cell line from FXS donor (male)	Maija L. Castrén laboratory	Not commercially available
Human iPSC-derived HEL69.6 cell line from FXS donor (male)	Maija L. Castrén laboratory	Not commercially available

(*Continued on next page*)

Continued

REAGENT or RESOURCE	SOURCE	IDENTIFIER
Human iPSC-derived HEL70.3 cell line from FXS donor (male)	Maija L. Castrén laboratory	Not commercially available
Human iPSC-derived HEL70.6 cell line from FXS donor (male)	Maija L. Castrén laboratory	Not commercially available
Human iPSC-derived HEL100.1 cell line from FXS donor (male)	Maija L. Castrén laboratory	Not commercially available
Human iPSC-derived HEL100.2 cell line from FXS donor (male)	Maija L. Castrén laboratory	Not commercially available
Human iPSC-derived microglia from healthy donor (male)	Jari Koistinaho laboratory	Not commercially available
Experimental models: organisms/strains		
C57Bl/6J wild type mice	Charles River Laboratories	C57BL/6NCrl; RRID: IMSR_CRL:027
Fmr1 KO mice (B6.129P2-Fmr1tm1Cgr/J)	Laboratory of Neurobiology, HiLIFE, University of Helsinki, Finland	RRID: IMSR_JAX:003025
Oligonucleotides		
Primers for gene expression analysis (SYBR Green qRT-PCR), see Table S1		
Software and algorithms		
AvidNote	Avidemic AB	https://avidnote.com
Bioconductor	Amezquita et al.[83]	https://doi.org/10.1038/s41592-019-0654-x
BioRender	Science Suite Inc.	https://www.biorender.com
Cell Ranger	10X Genomics	https://www.10xgenomics.com/support/software/cell-ranger/latest
DESeq2	Love et al.[84]	https://bioconductor.org/packages/release/bioc/html/DESeq2.html
GPT-5	OpenAI	https://chatgpt.com
GraphPad Prism	GraphPad	Version 11.0.0 (93)
GSDS	Hu et al.[85]	https://github.com/DimitriMeistermann/GSDS
Harmony	Korsunsky et al.[86]	https://doi.org/10.1038/s41592-019-0619-0
HCImage	HCImage	https://hcimage.com
ImageJ	National Institutes of Health	https://imagej.net/ij/
JASPAR	Baydar et al.[87]	https://jaspar.elixir.no
LIMSA	Haimi et al.[88]	https://github.com/RASpicer/MetabolomicsTools/blob/master/tools/LIMSA.md
MassHunter Qualitative Navigator	Agilent	https://www.agilent.com/en/product/software-informatics/mass-spectrometry-software/data-analysis/qualitative-analysis?srsltid=AfmBOooaJP36Pv0pWnl1_8DYIN0vgA_jnRUzvjSlw4DmNGR_CsulX5UE
MATLAB	MathWorks	https://www.mathworks.com/products/matlab.html
oob R package	Meistermann[89]	https://github.com/DimitriMeistermann/oob
Progenesis Qi	Nonlinear Dynamics	RRID:SCR_018923
R v4.3.2	R Foundation for Statistical Computing	Version 4.3.2
RStudio 2024.12.1 (Build 563)	Posit Software, PBC	Version 2024.12.1
STAR Aligner v2.5.0b	Dobin et al.[90]	https://github.com/alexdobin/STAR/releases/tag/2.5.0b
TriMap	Amid & Warmuth[91]	https://arxiv.org/abs/1910.00204

(*Continued on next page*)

Continued

REAGENT or RESOURCE	SOURCE	IDENTIFIER
Other		
SDS-PAGE 4–20% Mini-protean TGX gels	Bio-Rad	Cat# 456-1094
Trans-Blot Turbo Midi 0.2 μm PVDF Transfer Packs	Bio-Rad	Cat# 1704157
Trans-Blot Turbo Transfer system	Bio-Rad	Cat# 1704150

EXPERIMENTAL MODELS AND STUDY PARTICIPANT DETAILS

Human astrocytes

Differentiation of male FXS (HEL69.5, HEL69.6, HEL70.3, HEL70.6, HEL100.1 and HEL100.2) and control (HEL23.3, HEL24.3, HEL46.11, PO2/UEF-3A and PO4/UEF-3B) hiPSCs was performed as described previously.[30] Skin biopsies and blood samples were obtained from boys diagnosed with FXS (age range 6–13 years) for generation of the hiPSC cell lines after informed consent at Biomedicum Stem Cell Center (University of Helsinki, Finland). The research using human cells was approved by the Ethics Committee of the Hospital District of Helsinki and Uusimaa, Finland (permits 25/13/03/2011 and HUS/2951/2019).

FXS and control hiPSCs were maintained on Matrigel-coated plates in Essential 8 medium (E8; A1517001, Thermo Fisher Scientific Ltd.). For differentiation, 80% confluent hiPSCs were dissociated with 0.5 M ethylenediaminetetraacetic acid (EDTA; AM9260G, Invitrogen) and plated on low-attachment six-well plates in E8 with 20 ng/mL human basic fibroblast growth factor (bFGF2; 100-188, Peprotech) and 20 μM Rho kinase inhibitor (Y-27632 dihydrochloride (Y0503, Sigma-Aldrich). Neural induction occurred during 0–12 DIV on low-attachment plates in neuronal induction medium (NIM) containing 1% of each N2 supplement (17502048), Glutamax (35050061), non-essential amino acid supplement (NEAA; 11140050) and penicillin/streptomycin (P/S; 15070063) in Advanced Dulbecco's Modified Eagle Medium (DMEM/F12; 12634028) (all from Thermo Fisher Scientific). Advanced DMEM/F12 contains AlbuMAX II lipid-rich bovine serum albumin, which includes ALA, LA, oleic acid, stearic acid and PA, which allows cell culture without serum. Neural induction and patterning were achieved with 0.1 mM LDN-193189 (1062368, Stemgent), 1 mM cyclopamine (C4116, Sigma-Aldrich), 10 mM SB-431542 (S4317, Sigma-Aldrich) and 0.5 mg/mL DKK1 (Dickkopf-related protein 1; 120–30, Peprotech). Medium was changed twice a week. At 12 DIV, the medium was replaced by neuronal induction medium (NIM) supplemented with 20 ng/mL BDNF (450-02, Peprotech). At 30 DIV medium was changed to neurosphere medium (NS) containing 2% both B27-RA (12587010) and heparin (H4784), 1% of each Glutamax, NEAA and P/S in Advanced DMEM/F12 (all from Thermo Fisher Scientific). Differentiation and proliferation were sustained with 20 ng/mL both bFGF2 and epidermal growth factor (EGF; AF100-15, Peprotech). Embryoid bodies were manually dissociated once a week. At 60 DIV, spheres were dissociated and progenitors plated on culture plates coated with poly-ornithine (82682-33-5, Sigma-Aldrich) and laminin (114956-81-9, Sigma-Aldrich) in NS supplemented with 20 ng/mL CNTF (450-13, Peprotech). Cells were passaged with 0.05% Trypsin-EDTA (25300062, Thermo Fisher Scientific) approximately once a week and seeded at 20,000 cells/cm^2. Medium was changed twice a week. After 75 DIV, cells had acquired astrocyte morphology, and they were maintained on Matrigel-coated culture plates. ATRA (R2625, Sigma-Aldrich) was added to the culture medium as indicated.

Human microglia

Human microglia were differentiated from hematopoietic stem cells (HPCs) generated from hiPSCs (PO2 cell line) using StemDiff Hematopoietic kit (05310, StemCell Technologies) as previously described.[92,93] Briefly, hiPSC colonies were detached with ReLeSR (100-0483, StemCell Technologies), and 20–30 aggregates per well were plated on Matrigel-coated six-well plates in E8 medium with ROCK-inhibitor (Y-27632, Sigma). From the following day, well-distributed hiPSC colonies were cultured in StemDiff Medium, which was changed every other day, until HPCs appeared. After collection, 100,000–200,000 of non-adherent cells were seeded on a Matrigel-coated six-well plate with iMGL differentiation medium [DMEM/F12 (11320033, Gibco) supplemented with 2% Insulin-Transferrin-Selenium (ITS-G), 2% B27, 2 mM Glutamax, 1% NEAA, 0.5% N2 supplement, 0.5% P/S (all from Invitrogen), 5 μg/mL insulin (Sigma), 400 μM monothioglycerol (Sigma), 100 ng/mL IL34, 50 ng/mL Transforming Growth Factor β 1 (TGF-beta-1) and 25 ng/mL macrophage colony stimulating factor 1 (M-CSF) (all from Peprotech)]. Half of the medium volume was changed every other day until days 10–14 of differentiation. At days 10–14, the excess medium from the wells was centrifuged for 4 min at 300g to collect the floating microglial precursors, which were then placed back on the same plate, and 1 mL of the fresh iMGL Differentiation medium was added. The cells were fed with 1 mL/well of the medium every other day for 21–26 days. For microglia maturation, the cells were grown three additional days in iMGL maturation medium, which was formulated by supplementing iMGL differentiation medium with 100 ng/mL CX3CL1 (PeproTech) and 100 μg/mL CD200 (Biolegend). Differentiated microglia on Matrigel-coated 24-well plates were treated with *n*-6 DPA complexed with bovine serum albumin (BSA) (44502, Cayman Chemical), BSA-Fatty Acid Complexes (34932, Cayman Chemical) or ACM as indicated.

Mouse plasma samples

Fmr1 KO mice (B6.129P2-Fmr1tm1Cgr/J (JAX strain 003025; The Jackson) and C57Bl/6J wild type mice (Charles River Laboratories, USA) were used at the age of P14–15 in the study. Mice were housed under standard laboratory conditions and a 12 h dark-light cycle in the Animal Center of the University of Helsinki following the guidelines of the National Institutes of Health. All animal work was conducted under the approval of the *Guide for the Care and Use of Laboratory Animals*, the European Economic Community Council Directive and the National and the University Helsinki Research Ethics Committees on Animal Research (internal permit #KEK 24-016). KO mice were generated by crossing KO parents, and the female mice were littermates of the male mice. Blood samples were collected into EDTA-coated test tubes (030204, Kabe Labortechnic Gmbh) from the pups deeply anesthetized with isoflurane. After centrifugation at 4 °C for 15 min at 3,000 rpm, plasma was collected and stored at −70 °C until use.

METHOD DETAILS

Immunocytochemistry

For astrocyte marker analysis,[30] cells were plated on ViewPlate-96 (PerkinElmer) with 5,000 cells/well and two days later fixed with 4% paraformaldehyde for 15 min at room temperature (RT) followed by washing three times with phosphate buffered saline (PBS). Blocking with 10% normal goat serum and 0.05% Triton X-100 in PBS for 1 h preceded incubation with primary antibodies chicken anti-GFAP (4674, 1:1000; Abcam), mouse anti-S100B (S-2532, 1:500; Sigma-Aldrich) and rabbit anti-NF1A (39397, 1:500; Activ Motif) overnight at 4 °C. Secondary antibodies were Alexa Fluor 488 goat anti-chicken, Alexa Fluor 546 goat anti-rabbit and Alexa Fluor 635 goat anti-mouse (1:500; Invitrogen). The cells were imaged with Thermo Scientific CellInsight instrument.

Cell viability assay

For the viability assay,[94] 5,000 cells were plated per well on a 96 well-plate, and after two days culturing cells were treated with either dimethyl sulfoxide (DMSO) or ATRA for 24 h at 37 °C in a humidified atmosphere of 5% CO_2. On the following day, 3-(4,5-dimethyl-2-thiazolyl)-2,5-diphenyl-2H-tetrazolium bromide (MTT, M5655; Sigma-Aldrich) was added in the final concentration of 0.5 mg/mL. After incubation for 2 h at 37 °C, cells were lysed overnight with 100 μL MTT lysis buffer (20% sodium dodecyl sulfate in 50% *N,N*- dimethylformamide, pH 4.7) and the fluorescence was measured in a spectrophotometer at A_{570}.

Bulk RNA sequencing

The previously published RNA sequencing dataset (Gene Expression Omnibus database under accession number GSE228378) of cells at defined time points during astrocyte differentiation of isogenic control (H1) and FXS (*FMR1*KO) hPSCs[28,30] was used to explore reactivity marker expression. The sequencing reads were filtered based on quality and length, and after adapter removal the reads were aligned to the human genome using Star Aligner (version 2.5.0b)[90] and counted with high-throughput sequencing. Differential expression analysis was performed with the R package DESeq2.[84]

Astrocyte conditioned medium (ACM)

For medium collection from astrocyte cultures, cells were plated on Matrigel-coated T25 flasks at a density of 20,000 cells/cm^2 and grown for 7 days. On the day prior to the sample collection, the medium was replaced with 5 mL of fresh NS. As indicated cells were treated with 10 μM ATRA for 24 h. Collected medium was filtered through a 0.22 μm filter and stored at −80 °C until use.

LC-MS/MS untargeted lipidomics of astrocyte media

LC-MS/MS lipid analysis of human ACM was performed in the Metabolomics Core Facility at the University of California Riverside, USA, as described previously.[95,96] Analysis was performed on a Waters G2-XS quadrupole time-of-flight mass spectrometer coupled to a Waters Acquity I-class UPLC system. Separations were carried out on a Waters CSH C18 column (2.1 × 100 mm, 1.7 μM) and using a solvent gradient which started from 90% of phase A (60:40 acetonitrile:water) and increased the proportion of phase B (90:10 isopropanol:acetonitrile) from 10 to 99%. Both solvents contained 10 mM ammonium formate and 0.1% formic acid.[95] The flow rate was 400 μL/min and the column was held at 65 °C. The MS scan range was from 50 to 1600 m/z with a 100 ms scan time. MS/MS spectra were acquired in a data-dependent fashion. Ion source and desolvation temperatures, gas flows and capillary voltages were as described before.[68] A quality control sample, generated by pooling equal aliquots of each sample, was analyzed periodically to monitor system stability and performance. Injection volume of six μL was used for data acquisition. Analysis of the samples was performed in random order, and infusion of leucine enkephalin was used for mass correction.

Untargeted data processing (peak picking, alignment, deconvolution, integration, normalization and spectral matching) was performed in Progenesis Qi software (Nonlinear Dynamics). The analysis focused on FFAs and TGs in the medium samples, and the data were normalized to total ion abundance of sample or total abundance in the lipid class of interest. Lipids were identified according to the match of MS and MS/MS m/z values and retention time to an in-house database generated with authentic standards or by using external databases, the Lipidblast *in silico* database[97] and several mass spectral metabolite libraries in Mass Bank of North America, Metlin.[98] Details of the lipid identification, annotation and quality control procedures have been published before.[68]

LC-MS/MS untargeted lipidomics of astrocytes

Total lipids from differentiated astrocytes derived from 3 male FXS (HEL69.6, HEL70.6 and HEL100.2) and 4 control (HEL23.3, HEL24.3, PO2 and PO4) hiPSC lines were extracted as described by Folch et al.[99] Prior to the LC-MS/MS analysis, the solvents of the chloroform extracts were removed under nitrogen stream, the lipids were immediately redissolved into the initial LC mobile phase (45 μL of isopropanol/methanol 1:1) and the internal standard mixture (SPLASH® LIPIDOMIX® and Cer 18:1;O2/17:0, both from Avanti Polar Lipids, Alabaster, AL, USA) was added. Chromatographic separation was performed using an Agilent 1290 Infinity HPLC system equipped with a Luna Omega C18 100 Å (50 × 2.1 mm, 1.6 μm) column (Phenomenex) and using a solvent gradient which started from 68% of phase A (60:40 acetonitrile:water) and increased the proportion of phase B (90:10 isopropanol:acetonitrile) from 32 to 97%.[100] Both solvents contained 10 mM ammonium formate and 0.1% formic acid. The flow rate was 0.200 mL/min and column temperature 25 °C. The column eluent was infused into the electrospray source of an Agilent 6490 Triple Quad LC/MS with iFunnel Technology and spectra were recorded using both positive and negative ionization modes. The phospholipids were detected using head group specific precursor ion scans (PIS) or neutral loss (NL) scans: phosphatidylcholine diacyl (PC) and alkyl-acyl (PC O) and sphingomyelin (SM) species by PIS 184, phosphatidylethanolamine diacyl species (PE) by NL141, phosphatidylinositol species by PIS 241 and phosphatidylserine (PS) by NL87. Exceptionally the PE plasmalogens (PE P), giving weak NL 141 signal, were detected using MS- scan. Ceramides (Cer) were detected using sphingosine-specific PIS 264. TGs and cholesteryl esters (CE) were detected as $(M + NH_4)^+$ ions from MS + scan. The mass spectra were processed using MassHunter Qualitative Navigator software (Agilent) and the lipid species were quantified utilizing the internal standards and LIMSA software.[88] Lipid data are expressed as molar percentages (mol%) and lipid species are marked as follows: [sum of acyl chain carbons]: [sum of acyl chain double bonds] (e.g., PC 36:1) and for sphingomyelin [sum of sphingoid base and acyl chain carbons]: [sum of sphingoid base and acyl chain double bonds] (e.g., SM 34:1;O2).

FA structures in the astrocyte media were additionally confirmed by gas chromatography-mass spectrometry (GC-MS) using Shimadzu GCMS-QP2010 Ultra (Shimadzu, Kyoto, Japan). For example, the *n*-3 DPA and *n*-6 DPA were identified based on the diagnostic alpha and omega ions: m/z 208 and 108 for *n*-3 DPA and m/z 166 and 150 for *n*-6 DPA, respectively.[101]

GC-FID and GC-MS of mouse plasma FAs

Plasma samples from two pups of the same sex and from the same litter were combined to obtain sufficient material to include trace-level FAs into the FA compositions. As a result, the material included 3 WT male, 4 *Fmr1* KO male and 4 *Fmr1* KO female samples. First, the collected plasma samples (60–160 μL) were spiked with an internal standard (20 μg of FA 13:0) to allow calculating their total FA concentrations. It was found that the sampling protocol provided comparable samples since the total FA concentrations for the three study groups were similar (means 2.1–2.2 with SD 0.1–0.2 μg/μL). Next the standardized plasma samples were transferred into a solution of 1 mL hexane and 2 mL 1% H_2SO_4 in methanol and heated for 120 min at 95 °C in nitrogen atmosphere, which converted the FAs to FA methyl esters (FAMEs). The resulting FAME mixtures were extracted into hexane, and the solutions were dried on anhydrous Na_2SO_4 and concentrated under nitrogen flow for gas chromatography. The structures of the detected 58 individual FAMEs (and 5 dimethylacetals, derivatives of alkenyl chains of plasmalogen phospholipids) were identified using GC-MSD (Shimadzu GCMS-QP2010 Ultra) and comparing the mass spectra with those of the authentic standards (Supelco CRM47885, 47033, 47085-U, 47015-U and 47080-U) and published reference spectra.[102] Quantitative FA compositions were determined by GC-FID (Shimadzu GC-2010 Plus) by employing in the calculation theoretical response factors for FID,[103] and the accuracy and repeatability of the equipment response was monitored by a 37-component quantitative FAME standard (Supelco CRM47885). Subsequently, the corrected mass-based responses of the FAs were converted to mol% data by using their molar masses. Both GC systems were equipped with Zebron ZB-wax capillary columns (30 m, 0.25 mm ID and film thickness 0.25 μm; Phenomenex, Torrence CA, USA). Otherwise, the analyses were performed as described previously[104].

Single-cell RNA sequencing (scRNA-seq)

For scRNA-seq, control (PO2) and FXS (HEL69.5, HEL100.1) astrocytes were cultured on Matrigel-coated 3.5 cm culture plates. Cells were collected and prepared according to the Single Cell Analytics (SCA) General Cell Preparation Protocol of the University of Helsinki following the 10X Genomics recommendations.[105] Briefly, cells were rinsed with 0.5 mL of 1x PBS, treated with 0.05% Trypsin-EDTA solution for 3–5 min at 37 °C and centrifuged at 300g for 5 min at RT. After supernatant removal, cell pellet was dissolved in 1x PBS with 0.04% BSA. Cells were counted and partitioned using 10X Genomics Chromium Controller to capture up to 10,000 cells per sample, followed by reverse transcription, barcoding, complementary DNA (cDNA) amplification and library preparation. Obtained library was subsequently quantified by qRT-PCR and underwent next generation sequencing with Chromium Next GEM Single Cell 3′ Kit v3.1 (10X Genomics), according to manufacturer's instructions on Illumina NovaSeq 6000 system (Illumina). Raw base call file demultiplexing and generation of fastq files were performed using Cell Ranger mkfastq pipeline (10X Genomics). Sequencing depth targeted for each gene expression library and mean reads per cell were the following: 243,021,758 total reads with 18,581 reads per cell for PO2, 289,061,251 total reads with 25,832 reads per cell for HEL69.5 and 340,047,079 total reads with 34,186 reads per cell for HEL100.1.

Analysis of scRNA-seq data

The scRNA-seq was analyzed on the basis of the dedicated Bioconductor workflow.[83] Cells with less than 300 genes expressed were filtered out. A batch correction was performed between the 10X samples using Harmony.[86] A TriMap[91] 2D embedding was computed using the oob R package implementation[89]; oob contains wrappers that were used for data representation[106,107] and Leiden clustering[108]. Gene modules computation and functional enrichment were performed using GSDS.[85,109] Briefly, gene modules were detected using a Leiden clustering from a cosine distance matrix. Gene modules containing genes with minimal expression were discarded. The genes were then ordered within each module using the gene contribution to the activation score of the module (See GSDS documentation for more details[109]). The modules were renamed by the first transcription factor of the module. The transcription factor list was extracted from JASPAR.[87] Functional enrichment was performed by over-representation analysis using GO[110] and KEGG databases.[111]

RNA extraction and quantitative RT-PCR analysis

Total RNA was extracted from hiPSC-derived astrocytes (control cell lines: HEL23.3, HEL24.3 and PO2; FXS cell lines: HEL69.6, HEL70.6 and HEL100.2) and hiPSC-derived microglia using the RNeasy Mini Kit (74106; QIAGEN) according to the manufacturer's instructions and reverse-transcribed into cDNA using RevertAid H Minus Reverse Transcriptase (EP0451; Thermo Fisher Scientific). RT-PCR was performed using the PowerUp SYBR Green Master Mix (A25780; Thermo Fisher Scientific) and CFX Opus 96 Detection Systems (Bio-Rad) for 40 cycles of 95 °C for 15 s, 60 °C for 15 s and 72 °C for 1 min. Relative quantities of mRNA expression of the genes of interest were analyzed with the ΔΔCt method using *GAPDH* gene expression for normalization. The primers used to amplify the specific cDNA regions of transcripts are shown in Table S1. Each sample was run in triplicate with melting curve analysis to detect primer dimer artifacts.

Western blot analysis

The cells were lysed in the ice-cold Pierce™ RIPA buffer (89900; Thermo Scientific) with Pierce™ Protease (A32955; Thermo Scientific) and Pierce™ Phosphatase inhibitors (A32957; Thermo Scientific). After centrifugation at 4 °C and 9,000g for 15 min, the protein concentration of the supernatant samples was determined using Pierce BCA Protein assay kit (23255; Thermo Scientific). The protein extracts (10 mg), which were diluted in 2x loading buffer with b-mercaptoethanol, boiled at 95 °C for 7 min and cooled, were electrophoresed on SDS-PAGE 4–20% Mini-protean TGX gels (456–1094; Bio-Rad) and transferred to PVDF membranes using Trans-Blot Turbo Transfer system (1704150; Bio-Rad) and Trans-Blot Turbo Midi 0.2 μm PVDF Transfer Packs (1704157; Bio-Rad). The membranes were blocked in 5% non-fat dry milk in TBS, pH 7.4 (0.1 M Tris, 0.15 M NaCl) with 0.1% Tween 20 (TBST) for 1 h. The membranes were washed three times for 10 min in TBST. The incubation with rabbit anti-FATP1 (78571, 1:1000; Cell Signaling Technology) and mouse anti-GAPDH (MAB374, 1:2000; Sigma-Aldrich) diluted in BSA and NaN_3-containing blocking buffer overnight at 4 °C, was followed by washes in TBST and incubation with horseradish-peroxidase-conjugated secondary anti-mouse (A9044, 1:20,000; Sigma Aldrich) and anti-rabbit (A16096, 1:10,000; Invitrogen) IgG antibodies for 1 h at RT. Chemiluminescence detection was performed using the Pierce™ ECL Plus kit (32132; Thermo Scientific). Data were analyzed using NIH ImageJ software.

Calcium imaging

Calcium recordings on astrocytes were performed essentially as previously described.[23] For experiments, hiPSC-derived control and FXS astrocytes (50,000 per well) were plated on coverslips in a 12-well plate for imaging on the following day. ATRA-treated (10 μM, 24 h) and untreated cells were loaded with 4 μM Fura-2 (HB0780; HelloBio) in Hepes-buffered medium (pH 7.4) containing 137 mM NaCl, 5 mM KCl, 0.44 KH_2PO_4, 4.2 mM $NaHCO_3$, 1 mM $MgCl_2$, 1 mM $CaCl_2$ and 10 mM glucose (all from Sigma-Aldrich) at 37 °C for 30 min. The coverslip was then adjusted to SA-OLY/20 adapter and placed in the recording chamber with continuous perfusion with 37 °C Hepes-buffered medium (2 mL/min). ATP (100 μM) diluted in the buffer was added in the perfusion for 30 s during real-time imaging. Cells were excited with 340 and 380 nm wavelengths and the emission was recorded at 505 nm. Cell somas were outlined as regions of interest (ROIs), and $[Ca^{2+}]_i$ rise in each ROI was recorded. Using an Inverted IX70 microscope (Olympus Corporation)) cells were visualized with (UApo/340) ×10 air objective (Olympus) and images were captured with a Hamamatsu ORCA-Flash 4.0 camera. An image (ratio 340 nm/380 nm) was acquired each second, and up to 100 cells were recorded simultaneously. Data analysis was performed using HCImage and MATLAB.

QUANTIFICATION AND STATISTICAL ANALYSIS

The studies were performed using three FXS biological replicates generated from six different FXS hiPSC cell lines and three controls. Human microglia were differentiated from one control hiPSC line. For all data, the normality and homogeneity of variance were first analyzed. As indicated in figure legends, two-tailed *t* test and one-way analysis of variance (ANOVA) with Fisher's LSD test or Tukey's multiple comparisons test were performed using GraphPad Prism version 11.0.0 (93) and R version 4.3.2. The PCA was conducted using R version 4.3.2 and RStudio 2024.12.1 with packages factoextra, tidy verse and ggplot2.[112–114] Data are presented as mean ± SEM. Statistical significance was set to $p < 0.05$.